Arizona Geological Society Digest 22
2008

Geology and geochemistry of Jurassic plutonic rocks, Baboquivari Mountains, south-central Arizona

Gordon B. Haxel
U.S. Geological Survey, 2255 N. Gemini Dr., Flagstaff, Arizona, 86001, USA

Daniel J. May
Vice President for Academic Affairs, University of Findlay, Findlay, Ohio, 45840, USA

Thomas H. Anderson
Department of Geology and Planetary Sciences, University of Pittsburgh, Pittsburgh, Pennsylvania, 15260, USA

Richard M. Tosdal
Mineral Deposit Research Unit, Department of Earth and Ocean Sciences, University of British Columbia, Vancouver, British Columbia, Canada V6T 1Z4

James E. Wright
Department of Geology, University of Georgia, Athens, Georgia, 30602, USA

ABSTRACT

Among the plutons of the Jurassic magmatic arc segment in southern Arizona, northern Sonora, and southern California, two distinctive rock types dominate, occurring together in numerous mountain ranges: porphyritic, titanite-bearing hornblende-biotite granodiorite; and biotite leucogranite. These characteristic rocks are particularly well preserved and well exposed around Kitt Peak, in the Baboquivari Mountains, southern Arizona. The Middle to early Late Jurassic Kitt Peak Plutonic Suite (KPPS) comprises three units: Aguirre Peak Quartz Diorite (APQD; <170 Ma, ≥165 Ma, U-Pb), chiefly hornblende mesodiorite; Kitt Peak Granodiorite (KPGD; 165 Ma), hornblende-biotite granodiorite and monzogranite; and Pavo Kug Granite (PKG; 159 Ma), equigranular biotite leucogranite. This range also hosts a fourth, regionally unusual, Jurassic plutonic unit: the Baboquivari Peak Perthite Granite, related to post-arc, Late Jurassic crustal extension.

Binary variation diagrams, incompatible element patterns, and REE spectra indicate APQD and KPGD are consanguineous. APQD basaltic mesodiorite evidently approximates the parental magma for the APQD–KPGD series. More evolved rocks of this series evidently formed by combinations of fractional crystallization and mixing with or assimilation of crustal material. PKG is less directly related to APQD and KPGD than these two are to one another.

e-mail: Haxel: gbhaxel@usgs.gov; May: may@findlay.edu; Anderson: taco@imap.pitt.edu; Tosdal: rtosdal@eos.ubc.ca; Wright: jwright@gly.uga.edu

Haxel, G.B., May, D.J., Anderson, T.H., Tosdal, R.M., and Wright, J.E., 2008, Geology and geochemistry of Jurassic plutonic rocks, Baboquivari Mountains, south-central Arizona, *in* Spencer, J.E., and Titley, S.R., eds., Ores and orogenesis: Circum-Pacific tectonics, geologic evolution, and ore deposits: Arizona Geological Society Digest 22, p. 497–515.

JURASSIC PLUTONIC ROCKS IN THE BABOQUIVARI MOUNTAINS: HISTORICAL AND REGIONAL CONTEXT

Before about 1980, a principle of southern Arizona geology seemed to be "Unless proven otherwise, igneous rocks are Laramide" (that is, Late Cretaceous to early Paleogene in age). This rule is evident in 1960s county and state geologic maps (e.g., Wilson, 1960; Wilson et al., 1960, 1969; Cooley, 1967). Some of these maps even have units such as Lgr—Laramide granite. Assignment of default Laramide ages to igneous rocks persisted despite gathering evidence to the contrary. Post-Paleozoic, pre-Cretaceous plutons had been recognized as early as 1904, near Bisbee (Ransome, 1904; Gilully, 1956). In the 1950s through 1970s, igneous rocks mapped in several ranges west of Bisbee were identified as early to middle Mesozoic, Triassic, or Jurassic (e.g., Cooper, 1971; Drewes, 1971, 1976). However, corroborating isotopic ages were not forthcoming because the only geochronologic methods applied were K-Ar and Pb-α. Likewise, undated or poorly dated early to middle Mesozoic igneous rocks were identified over wide areas of western Arizona (Reynolds, 1980).

By the late 1970s, a growing database of U-Pb isotopic ages from northern Sonora and southern and western Arizona (Silver, 1974; Dillon, 1975; Anderson and Silver, 1978; Haxel et al., 1980b; Reynolds et al., 1987) showed that many igneous rocks that were presumed Laramide or could be assigned only vague early to middle Mesozoic ages are in fact ≈ 175–145 Ma, Middle to Late Jurassic. This discovery led in turn to recognition of a major new tectonic element in Arizona geology: a Jurassic magmatic arc segment extending from southern Arizona and northern Sonora westward into southern California (Coney, 1978; Tosdal et al., 1989; Anderson et al., 2005). The diverse igneous rocks of this arc segment range from ultramafic hornblendite to high-silica leucogranite and rhyolite, from calcalkaline to distinctly alkaline, and from metaluminous to weakly peraluminous.

Some of the best preserved, best exposed, and most accessible examples of Jurassic plutonic rocks in southern Arizona and northern Sonora crop out in the northern Baboquivari Mountains, around Kitt Peak National Observatory (Sage and Ashenbrenner, 2003), 65 km southwest of Tucson (Fig. 1). Numerous roadcuts and natural outcrops in canyons along the road that ascends 1100 m to the mountain-top observatory provide excellent exposures of 165 Ma, porphyritic, titanite-bearing hornblende-biotite granodiorite. This distinctive granodiorite is the single most abundant plutonic rock type within the Jurassic arc segment. Similar granodiorite of the same age occurs as far west as the San Gabriel Mountains, north of Los Angeles (Barth, 1990). One section of the Kitt Peak road provides exposures of biotite leucogranite, another characteristic rock type within the Jurassic arc. Dioritic rocks parental to the granodiorite and granite crop out elsewhere in the Baboquivari Mountains. This range also is home to a fourth, and regionally unusual, type of Jurassic plutonic rock: perthite granite and quartz-perthite syenite. This unit postdates the main phase of arc magmatism and is related to Late Jurassic crustal extension.

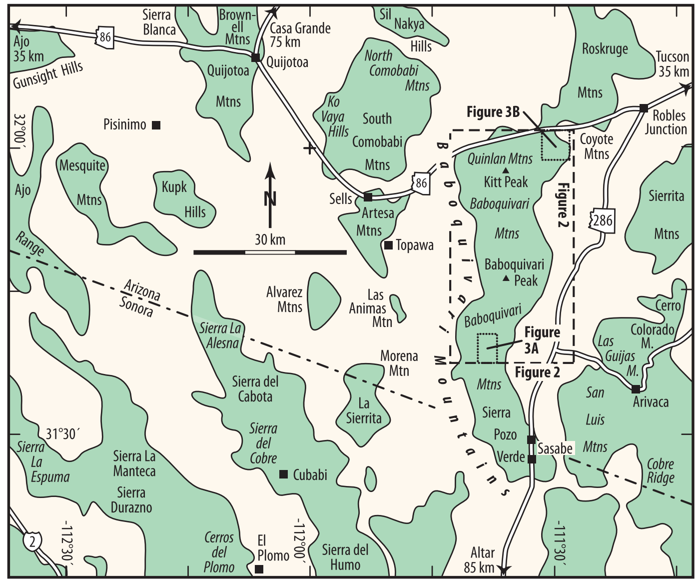

Figure 1. Regional setting of the Baboquivari Mountains, south-central Arizona and north-central Sonora. Mountains, hills, and other areas of bedrock outcrop (Richard, et al., 2000; Anderson et al., 2005; Anonymous, no date) are mapped in green. Ranges labeled in italic are those from which Jurassic U-Pb isotopic ages have been determined (Table 1). "Baboquivari Mountains" as used herein includes four contiguous and geologically coherent ranges: Sierra Pozo Verde, Baboquivari Mountains proper, Quinlan Mountains, and Coyote Mountains. The next range to the north, the Roskruge Mountains, is lower and geologically distinct (Ferguson et al., 2000).

In this paper we present the first petrologic study of the Jurassic plutonic rocks of the Baboquivari Mountains, combining information from geologic mapping and petrography circa 1978–1982 with modern analytical data for a comprehensive suite of major and trace elements. After describing the geologic setting and petrography of the plutonic rocks and summarizing their U-Pb ages, we consider their classification in term of major elements, their trace element characteristics, and their petrogenesis.

GEOGRAPHIC SETTING, GEOLOGIC FRAMEWORK, AND GEOLOGIC HISTORY OF THE BABOQUIVARI MOUNTAINS

The Baboquivari Mountains are actually a chain of several ranges, separately named but contiguous and geologically coherent (Fig. 1). This chain extends some 80 km, from Sierra Pozo Verde straddling the Sonora-Arizona border, through the highest part of the Baboquivari Mountains proper around Baboquivari Peak, to the Quinlan Mountains around Kitt Peak. The small but rugged Coyote Mountains, northeast of Kitt Peak, are geologically continuous with the Kitt Peak area and can be considered an extension of the Quinlan and northern Baboquivari Mountains. We shall generally use the single name *Baboquivari Mountains* to refer collectively to these four closely related ranges.

Like the rest of southern Arizona, the Baboquivari Mountains region is underlain by Paleoproterozoic continental crust (Farmer and DePaolo, 1984; Asmerom et al., 1991; Lang and Titley, 1998: Bouse et al., 1999). However the Baboquivari Mountains lie within an anomalous region, the Papago domain, where virtually no autochthonous Proterozoic basement rocks are exposed (Haxel et al., 1984; Riggs and Haxel, 1990; Tosdal et al., 1990; Nourse et al., 1994; Anderson et al., 2005). The oldest rocks of known age in the Baboquivari Mountains are metamorphosed Paleozoic strata restricted to a few small rafts within an early Paleogene pluton (Carrigan, 1971).

Jurassic rock units of the Baboquivari Mountains

Most of the Baboquivari Mountains is composed of Jurassic sedimentary, volcanic, hypabyssal, and plutonic rocks (Fig. 2) (Haxel et al., 1980a, 1982, 2005; Beikman et al., 1995). The oldest unit is the Middle Jurassic (170 Ma) Topawa Group, comprising a volcanic and sedimentary sequence about 8 km in stratigraphic thickness plus related hypabyssal porphyry intruding the lower part of the sequence. Topawa Group rocks make up much of the crest and west side of the northern and central Baboquivari Mountains. Southward, the Topawa Group grades into derivative metamorphic rocks of the Chutum Vaya Complex, which occupies the entire width of the range south of a transverse structure, the Osobavi fault, south of Baboquivari Peak (Goodwin and Haxel, 1990).

The Topawa Group is intruded by the Middle to Late Jurassic, mafic to silicic plutonic rocks described in this paper. Geologic mapping, supported by U-Pb geochronology, petrography, and whole-rock geochemistry, show that these plutonic rocks comprise four units (in order of decreasing age): Aguirre Peak Quartz Diorite (APQD), Kitt Peak Granodiorite (KPGD), Pavo Kug Granite (PKG), and Baboquivari Peak Perthite Granite (BPPG). APQD, KPGD, and PKG are genetically related and constitute the Kitt Peak Plutonic Suite (KPPS) (Fig. 2). Together, the Middle to early Late Jurassic Topawa Group and KPPS represent the main phases of Jurassic arc magmatism in this region (Tosdal et al., 1989; Anderson et al., 2005). In contrast, the BPPG is a member of the Late Jurassic Ko Vaya Suite (Haxel et al., 2008, this volume), generated by post-arc magmatism associated with crustal extension and transform faulting (Anderson and Nourse, 2005). PKG, of early Late Jurassic age, may be transitional between the arc and extensional phases.

Jurassic units peripheral to the Baboquivari Mountains

Three distinctive Late Jurassic units—Roadside Formation, Ko Vaya granite, and Sand Wells Formation—crop out in the western and northern foothills of the Baboquivari Mountains (Figs. 2, 3). These units have no counterparts within the main part of the Baboquivari Mountains, but closely resemble terranes that make up several nearby ranges to the west—Comobabi, Artesa, Quijotoa, and Brownell Mountains (Haxel et al., 1978, 1984; May and Haxel, 1980). The Roadside Formation and Ko Vaya granite are members of the aforementioned Ko Vaya Suite. These three peripheral units are separated from Jurassic rocks of the main Baboquivari Mountains by latest Cretaceous, Paleogene, or Neogene faults, interpreted by Haxel et al. (2008) as reactivated Late Jurassic faults.

Post-Jurassic units and episodes

In latest Cretaceous to early Paleogene time, an orogenic episode involving thrust faulting and regional metamorphism culminated in crustal melting that produced numerous stocks or small plutons of early Paleogene (≈ 58 Ma) peraluminous leucogranite (Wright and Haxel, 1982; Farmer and DePaolo, 1984; Haxel et al., 1984; Nourse et al., 1994). Such plutons crop out three places in the Baboquivari Mountains chain: Sierra Pozo Verde, western Quinlan Mountains, and Coyote Mountains. Each pluton is accompanied by a swarm or cluster of pegmatite, aplite, and granite dikes; pegmatite dikes are especially abundant in the central Coyote Mountains (Fig. 2).

The youngest major units of the Baboquivari Mountains are latest Paleogene, ≈ 24 Ma. They include two localized swarms of microdiorite and minette dikes; extensive swarms and networks of rhyolite dikes in the central part of the range; and a small volcanic field of rhyolitic domes, flows, and volcaniclastic rocks on the west side. All three units are petrogenetically related. The north and south ends of the Baboquivari Mountains are marked by latest Paleogene to early Neogene metamorphic core complexes, which make up most of Sierra Pozo Verde (Davis, 1980; Goodwin and Haxel, 1990) and the north slope of the Coyote Mountains (Gardulski, 1980; Wright and Haxel, 1982; Tosdal et al., 1990). These core complexes comprise lineated mylonites and mylonitic orthogneisses overlain along normal faults by unmetamorphosed rocks.

Metamorphism of Jurassic plutonic rocks

In four areas, Jurassic plutonic rocks are metamorphosed. Within the Chutum Vaya Complex, some APQD intrusions are converted to schist, but others retain igneous features (Figs. 2, 3A). In the Coyote and eastern Quinlan Mountains, APQD is partially converted to schist or fine-grained gneiss, and KPGD and PKG are pervasively foliated and densely intruded by pegmatite. In the northern Coyote Mountains, APQD is locally mylonitized (Fig. 3B). In the western Quinlan Mountain, PKG is locally foliated. Elsewhere in the Baboquivari Mountains Jurassic plutonic rocks generally bear little or no evidence of metamorphism.

Figure 2. Geologic map of the northern and central Baboquivari Mountains, emphasizing Middle and Late Jurassic plutonic rocks (after Haxel et al., 1980a, 1982, 2005; Beikman et al., 1995). Three major dike swarms and numerous small rhyolite intrusions, all Paleogene, are not shown. Location of this map is shown in Figure 1. Regarding the age of the Sand Wells Formation, see Haxel et al. (2008).

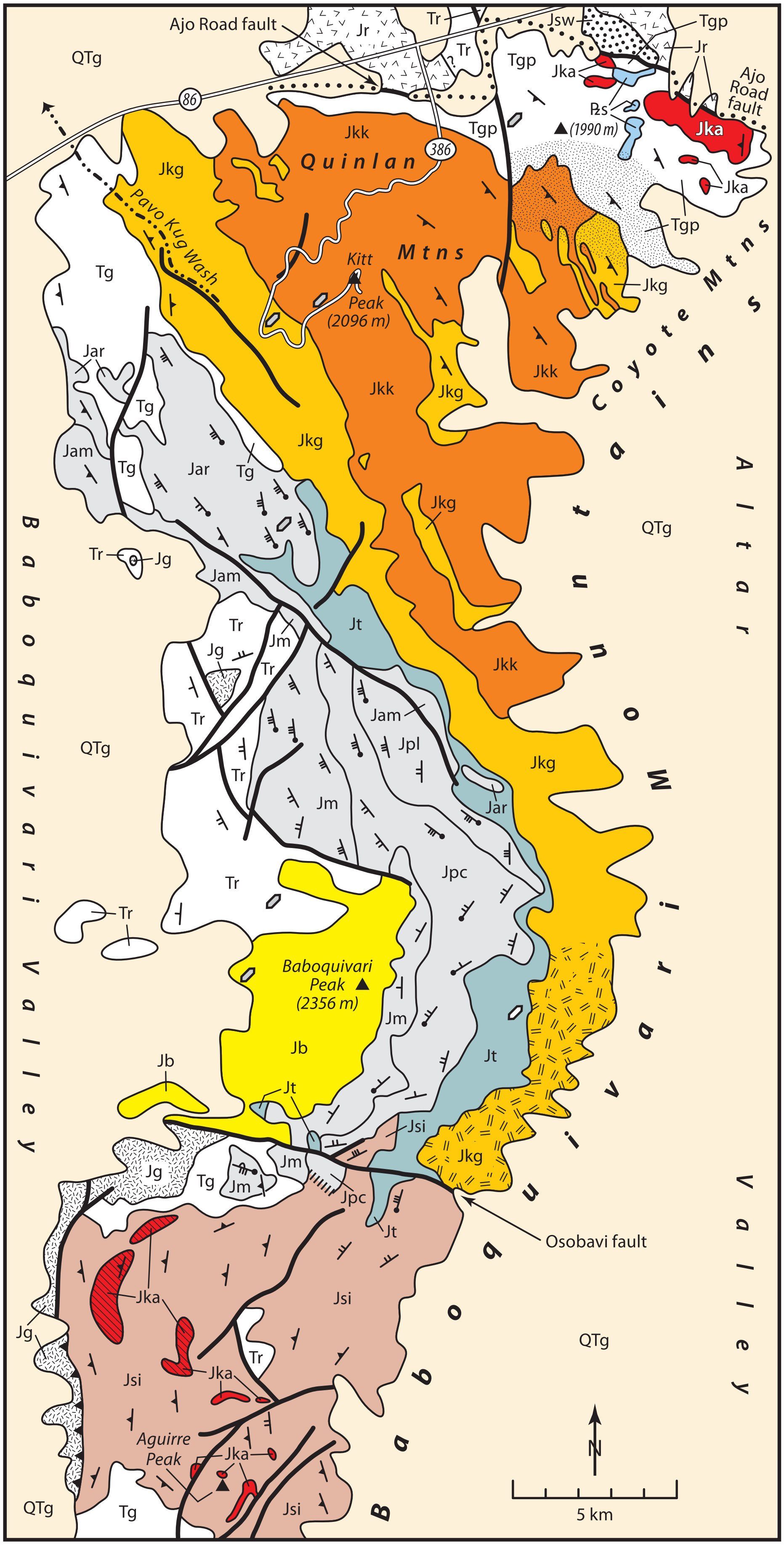

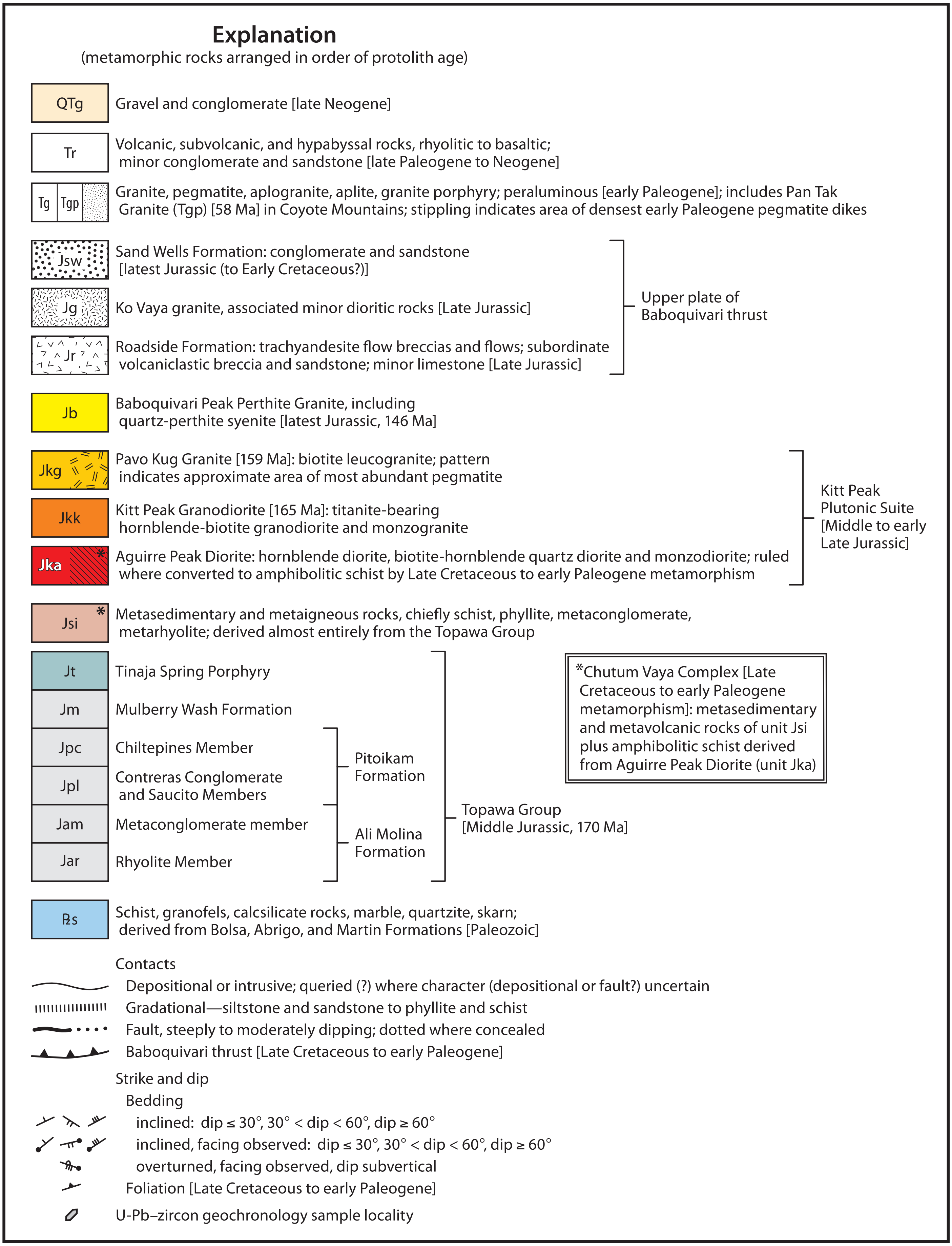
Explanation
(metamorphic rocks arranged in order of protolith age)
QTg
Gravel and conglomerate [late Neogene]
Tr
Volcanic, subvolcanic, and hypabyssal rocks, rhyolitic to basaltic; minor conglomerate and sandstone [late Paleogene to Neogene]
Tg
Tgp
Granite, pegmatite, aplogranite, aplite, granite porphyry; peraluminous [early Paleogene]; includes Pan Tak Granite (Tgp) [58 Ma] in Coyote Mountains; stippling indicates area of densest early Paleogene pegmatite dikes
Jsw
Sand Wells Formation: conglomerate and sandstone [latest Jurassic (to Early Cretaceous?)]
Jg
Ko Vaya granite, associated minor dioritic rocks [Late Jurassic]
Jr
Roadside Formation: trachyandesite flow breccias and flows; subordinate volcaniclastic breccia and sandstone; minor limestone [Late Jurassic]
Upper plate of Baboquivari thrust
Jb
Baboquivari Peak Perthite Granite, including quartz-perthite syenite [latest Jurassic, 146 Ma]
Jkg
Pavo Kug Granite [159 Ma]: biotite leucogranite; pattern indicates approximate area of most abundant pegmatite
Jkk
Kitt Peak Granodiorite [165 Ma]: titanite-bearing hornblende-biotite granodiorite and monzogranite
Jka *
Aguirre Peak Diorite: hornblende diorite, biotite-hornblende quartz diorite and monzodiorite; ruled where converted to amphibolitic schist by Late Cretaceous to early Paleogene metamorphism
Kitt Peak Plutonic Suite [Middle to early Late Jurassic]
Jsi *
Metasedimentary and metaigneous rocks, chiefly schist, phyllite, metaconglomerate, metarhyolite; derived almost entirely from the Topawa Group
Jt
Tinaja Spring Porphyry
Jm
Mulberry Wash Formation
Jpc
Chiltepines Member
Jpl
Contreras Conglomerate and Saucito Members
Pitoikam Formation
Jam
Metaconglomerate member
Jar
Rhyolite Member
Ali Molina Formation
Topawa Group [Middle Jurassic, 170 Ma]
*Chutum Vaya Complex [Late Cretaceous to early Paleogene metamorphism]: metasedimentary and metavolcanic rocks of unit Jsi plus amphibolitic schist derived from Aguirre Peak Diorite (unit Jka)
Ꝑs
Schist, granofels, calcsilicate rocks, marble, quartzite, skarn; derived from Bolsa, Abrigo, and Martin Formations [Paleozoic]
Contacts
Depositional or intrusive; queried (?) where character (depositional or fault?) uncertain
Gradational—siltstone and sandstone to phyllite and schist
Fault, steeply to moderately dipping; dotted where concealed
Baboquivari thrust [Late Cretaceous to early Paleogene]
Strike and dip
Bedding
inclined: dip ≤ 30°, 30° < dip < 60°, dip ≥ 60°
inclined, facing observed: dip ≤ 30°, 30° < dip < 60°, dip ≥ 60°
overturned, facing observed, dip subvertical
Foliation [Late Cretaceous to early Paleogene]
U-Pb–zircon geochronology sample locality

JURASSIC PLUTONIC UNITS: DISTRIBUTION, FIELD AND AGE RELATIONS, PETROGRAPHY, ISOTOPIC AGES

Aguirre Peak Quartz Diorite

APQD crops out in two widely separated areas: the southern Baboquivari Mountains, within the Chutum Vaya Complex; and the northern Coyote Mountains (Figs. 2, 3). In the former area, APQD intruded Topawa Group rocks, in Middle Jurassic time. Subsequently, in latest Cretaceous to early Paleogene time, the two units underwent regional metamorphism together. Around Aguirre Peak, where Topawa Group rocks were converted to phyllite and low-grade schist, APQD was resistant to metamorphism and igneous textures, minerals, and contacts are generally preserved. Farther northwest within the Chutum Vaya Complex, higher-grade metamorphism converted APQD intrusions to amphibolitic schist, obscuring or obliterating igneous features.

Igneous characteristics of APQD are best preserved in several small intrusions around and north of Aguirre Peak (Fig. 3A). Intrusions exposed in areas of relatively high relief appear pipe-like or irregular. Some intrusions are strongly heterogeneous in texture and composition, ranging from coarse-

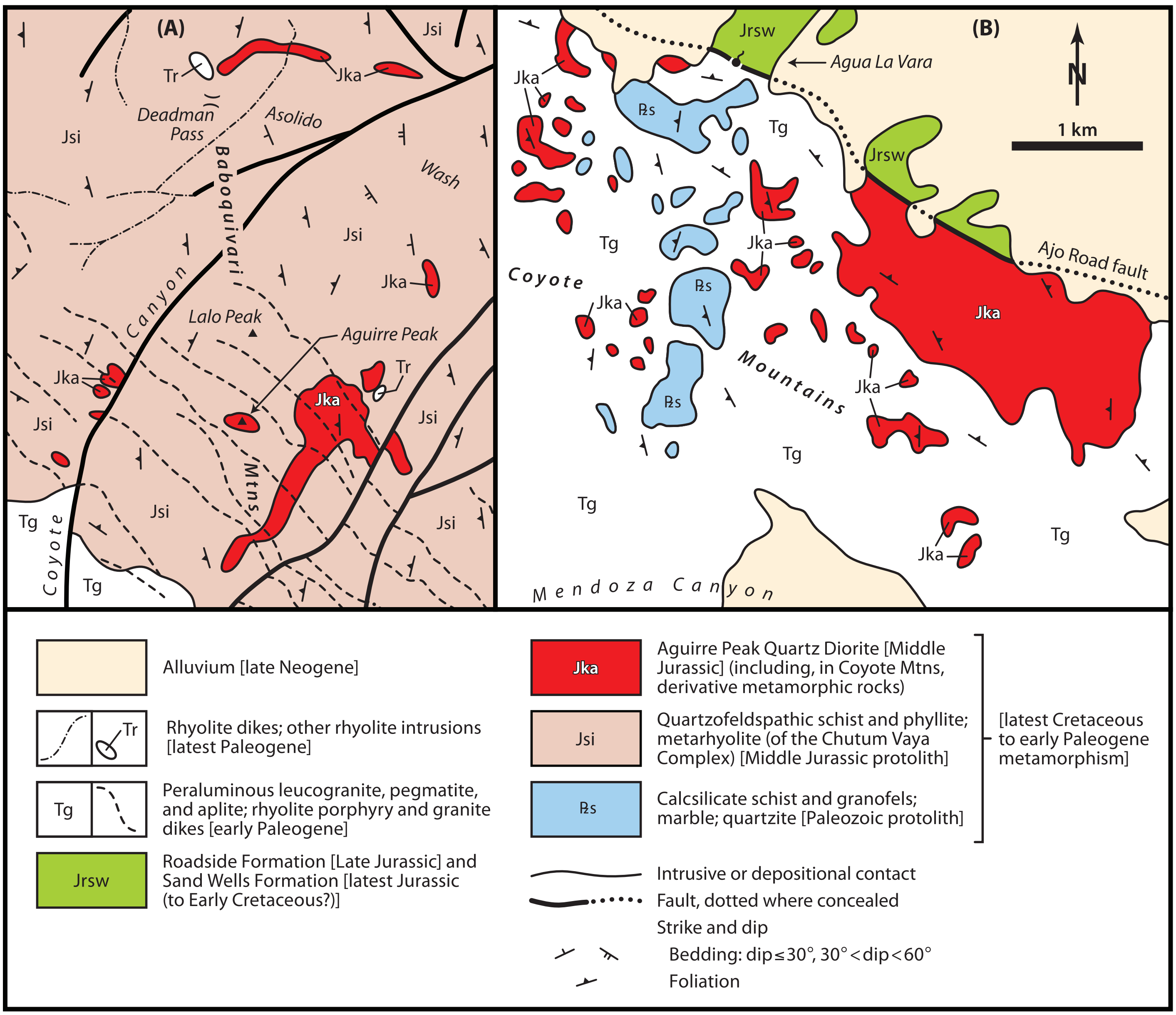

Figure 3. Generalized geologic maps of the Aguirre Peak Quartz Diorite: **(A)** around Aguirre Peak, southern Baboquivari Mountains (after Haxel et al., 1982) and **(B)** in the Coyote Mountains. Both maps have the same scale. In map B, voluminous pegmatite dikes are not shown (see Fig. 2). In the Coyote Mountains, early Paleogene (≈ 58 Ma) crystalloblastic foliation dips westward, whereas latest Paleogene (≈ 24 Ma) mylonitic foliation dips northward to northeastward (Wright and Haxel, 1982). Agua La Vara (map B) is a spring and abandoned well situated in the gouge zone of the Ajo Road fault. Location of these maps is shown in Figure 1.

grained melanodiorite to fine-grained leucodiorite (Fig. 4). Two varieties of dioritic rock are most common. The first, which crops out at and east and southeast of Aguirre Peak, comprises coarse- to medium-grained, mesocratic hornblende and augite-hornblende diorite and quartz diorite. Hornblende phenocrysts are typically blocky, subhedral to euhedral, and 5–15 mm across (Fig. 5A). Some have cores of augite or olivine. Mesodiorite locally grades into melanodiorite or, rarely, hornblendite. The second variety, which crops out in Coyote Canyon and north of Deadman Pass and Asolido Wash, is medium- to fine-grained mesocratic to leucocratic biotite-hornblende quartz diorite and quartz monzodiorite, equigranular or hornblende-phenocrystic.

In the Coyote Mountains, numerous rafts or blocks of APQD are spread out along the side or top of an early Paleogene leucogranite pluton (Fig. 3B). In some places these dioritic rocks have been converted to biotite-rich schist or, less commonly, fine-grained gneiss. In other places, however, they are only slightly metamorphosed and closely resemble the dioritic rocks around Aguirre Peak. The single largest mass, in the northeast Coyote Mountains, evidently is a heterogeneous dioritic stock, bigger than but otherwise similar to the intrusions in the southern Baboquivari Mountains. Some of the smaller blocks west and south of the large mass probably are fragments detached from this stock by intrusion of the leucogranite; others may represent smaller disrupted stocks, or may have been separate pipe-like intrusions. We found three additional minor or rare varieties of dioritic rock in the Coyote Mountains: pyrrhotite-bearing olivine hornblendite, magnetite-rich hornblende diorite (possibly a metasomatic rock), and dioritic pegmatite with large hornblende laths.

In the northern Coyote Mountains, APQD locally intrudes Paleozoic strata. In an area about 12 km south-southeast of Kitt Peak, several meter-size xenoliths of APQD occur within KPGD, indicating APQD is at least slightly older than KPGD. Geochemical and U-Pb geochronologic data, discussed in subsequent sections, indicate APQD and KPGD are consanguineous and broadly coeval.

Kitt Peak Granodiorite

KPGD crops out over an area about 9 by 21 km in the northern Baboquivari Mountains. All contacts are with younger intrusions or alluvium (Fig. 2), so the original shape and size of the Kitt Peak pluton are uncertain. Granodiorite identical or very similar to KPGD crops out in five other ranges in south-central Arizona and north-central Sonora (Fig. 1): Cobre Ridge (Knight, 1970), Morena Mountain, Cerros del Plomo, Sierra La Espuma, and Kupk Hills. Rare blocks or xenoliths of metagranite derived from KPGD occur within early Paleogene granite in at least three places in Sierra Pozo Verde, near Sasabe. Cobre Ridge and Sierra La Espuma lie about 65 and 105 km, respectively, from Kitt Peak. The subsurface extent of the Kitt Peak pluton, or several similar plutons, evidently is of batholithic dimensions (Anderson et al., 2005).

KPGD is fairly uniform in texture and grain size, but with some variation in feldspar ratios and color index (Fig. 4). Although the eight modal compositions determined for this unit plot equally between granodiorite and monzogranite, field observation indicates granodiorite is more abundant. Both rock types are relatively quartz-poor and locally grade into quartz monzodiorite or quartz monzonite. The predominant variety of KPGD is medium- to coarse-grained, titanite-bearing hornblende-biotite granodiorite (Fig. 5B). Pale-pink, -lavender, or -gray subhedral phenocrysts of alkali feldspar 2–4 cm long and millimeter-size, honey-colored, euhedral titanite crystals are identifying characteristics. Seriate or equigranular textures are locally common. Ragged aggregates of fine-grained, anhedral black biotite are typical. In many rocks, but not all, these aggregates partially replace hornblende.

Within KPGD, enclaves of fine-grained biotite-rich quartz monzodiorite—unfoliated to schistose, lenticular, and 5 cm to 2 m in largest dimension—are common. Given their uniformity and wide distribution, these enclaves probably are autholithic (cognate), not xenolithic. Veins of epidote with various combinations of quartz, hematite, tourmaline, albite, and pyrite (locally chalcopyrite) are sparse but widespread.

The general uniformity of KPGD has two exceptions. In the southwest Coyote Mountains, some KPGD is more mafic and appears transitional to APQD. In an indefinite area of at least several square kilometers about 5 or 6 km south-southeast of Kitt Peak, KPGD is more strongly porphyritic but titanite is less abundant or less conspicuous. Rock in this area may constitute a separate intrusive phase or sub-pluton.

Pavo Kug Granite

PKG makes up a narrow, arcuate belt, some 35 km long and a few kilometers wide, in the northern and central Baboquivari Mountains (Fig. 2). The western boundary of this body is, for most of its length, an intrusive contact with the Topawa Group. The northern half of the eastern boundary is an intrusive contact with KPGD. Both contacts are generally steep to subvertical. The tabular or slab-like form of the northern part of the Pavo Kug intrusion must be a primary feature; whether the arcuate shape of the western contact is primary or a product of later deformation is uncertain. In the southern one-quarter of its outcrop area, PKG is mostly pegmatite and pegmatoid granite (Fig. 2), probably forming the top of the pluton. Around and south of Kitt Peak and in the southern Coyote Mountains, numerous dikes, prongs, and bosses of PKG intrude KPGD. Most of the smaller dikes are pegmatite or aplite. Over much of their length, contacts between PKG and KPGD trend north-northwest. KPGD in Cobre Ridge is accompanied by granite similar to PKG. Distribution of PKG-like granite in Sonora remains uncertain.

PKG consists of texturally heterogeneous, coarse- to fine-grained, equigranular biotite leucogranite (monzogranite and syenogranite) (Figs. 4, 5C). Large, irregular to ovoid, gray quartz crystals with greasy luster are characteristic (Fig. 5C).

Biotite, typically 1–3 percent of the rock, forms either small, subhedral flakes or polycrystalline aggregates. Traces of titanite or allanite, rarely apparent in hand specimen, are found in a some thin sections. PKG generally lacks garnet or primary muscovite; minor fine-grained muscovite is deuteric or hydrothermal. Quartz monzodioritic enclaves, characteristic of KPGD, are virtually absent from PKG. Epidote veins are considerably less common than in KPGD.

Baboquivari Peak Perthite Granite

This unit forms a single stock, about 10 km in largest exposed dimension, that intrudes the upper Topawa Group

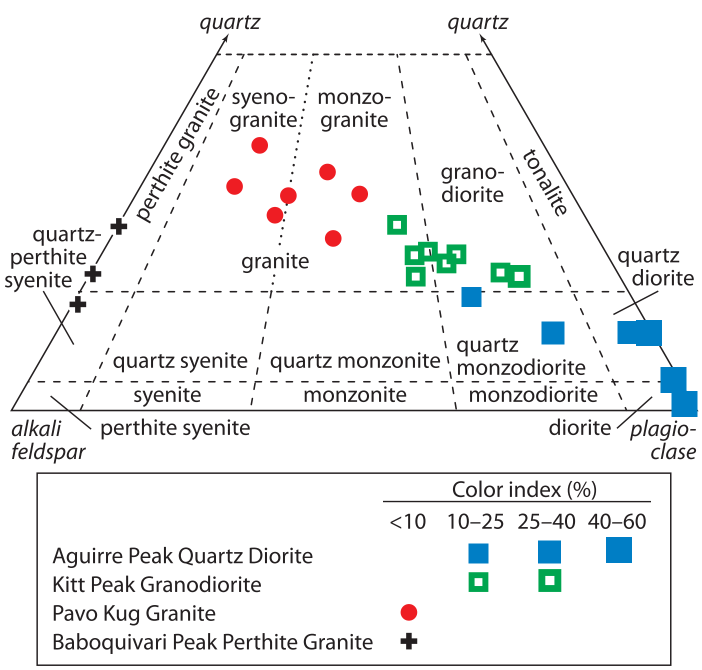

Figure 4. Modal compositions of Jurassic plutonic rocks, Baboquivari Mountains. Sizes of symbols indicate approximate color index (fraction of mafic minerals). Coarser-grained rocks were point counted using polished slabs and finer-grained rocks using thin sections, both stained for alkali feldspar.

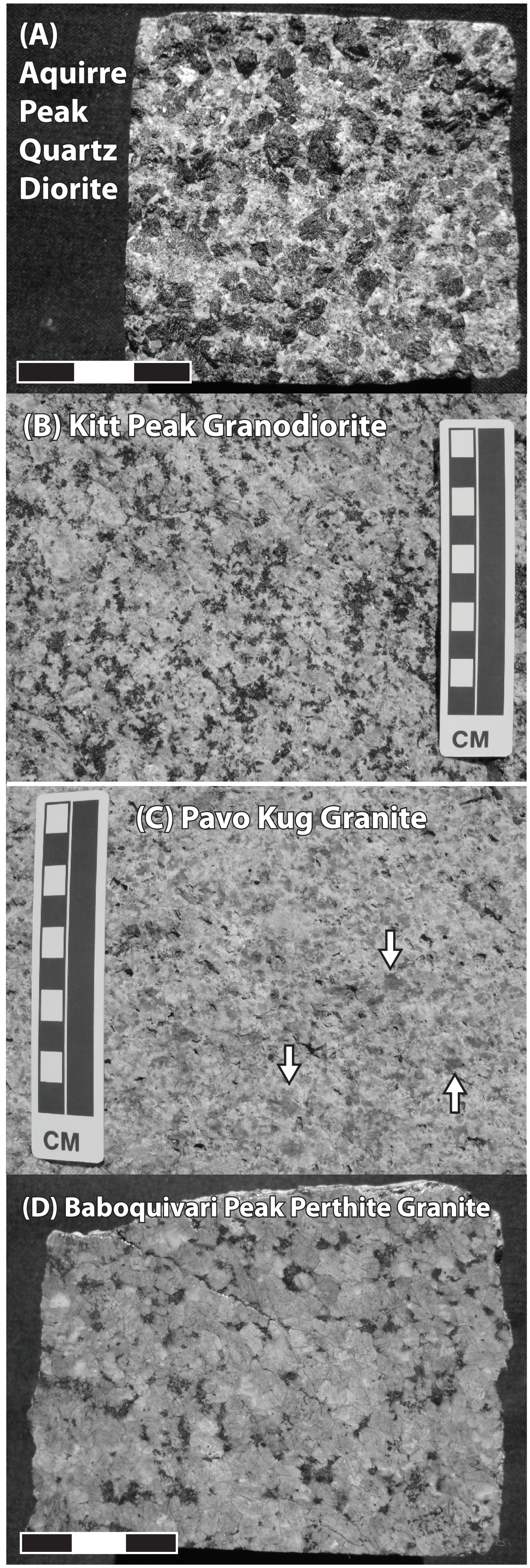

Figure 5. Typical outcrops and hand specimens of Jurassic plutonic rocks, Baboquivari Mountains. **(A)** APQD—medium-grained mesodiorite with blocky hornblende phenocrysts. Aguirre Peak. **(B)** KPGD—coarse-grained, sparsely porphyritic hornblende-biotite granodiorite, with ragged aggregates of biotite and subhedral phenocrysts of alkali feldspar (left side). Unweathered rock in roadcut on Kitt Peak. **(C)** PKG—weathered surface on coarse-grained, equigranular biotite leucogranite, showing characteristic medium-gray, ovoid to irregular quartz crystals (three examples are indicated by arrows). Southwest flank of Kitt Peak. **(D)** BPPG—perthite granite. In this photograph perthite and quartz overlap in albedo, possibly giving the impression of more quartz than is actually present (see Fig. 4). Dark material is a mixture of hematite and chlorite that has completely replaced the original mafic minerals. Lower Baboquivari Canyon. Scales in A and D represent 3 cm; in B and C, 10 cm.

around Baboquivari Peak. It is composed of red-brown to dusky-red, leucocratic perthite granite and quartz-perthite syenite (Figs. 4, 5D). BPPG is fairly homogeneous, medium- to coarse-grained, and typically equigranular but locally porphyritic. In some rocks quartz has a bluish cast. Accessory biotite, hornblende, or hastingsite are variably and often highly altered; alteration minerals locally include blue amphibole. Iron-oxide staining is pervasive. Some parts of the stock are silicified. BPPG is not genetically related to the other Jurassic plutonic rocks of the Baboquivari Mountains, the KPPS. The petrochemistry of BPPG is discussed along with that of the other members of the Ko Vaya Suite by Haxel et al. (2008).

Baboquivari Peak (2356 m) is a massive columnar to pyramidal tower of perthite granite sitting atop less resistant parts of the Baboquivari Peak stock. This peak rises some 1200 m above the pediments on either side of the range, and forms a regional landmark visible for many kilometers from every direction except north. The resistance to erosion of Baboquivari Peak seems to owe to semi-pervasive silicification of the granite.

Uranium-lead isotopic ages

For many of the major Jurassic igneous units of south-central Arizona and north-central Sonora, U-Pb zircon isotopic ages have been determined independently two or three times (Table 1): by T.H. Anderson in Sonora (Anderson and Silver, 1978; Anderson et al., 2005); by J.E. Wright in the Baboquivari Mountains region (Haxel et al., 1980b, 2005, 2008; Tosdal et al., 1989); and by N.R. Riggs (Riggs et al., 1993) and other geochronologists in the Arivaca region, Arizona. Variations of a few million years in the inferred ages of similar rock units probably reflect differing interpretations of slightly discordant U-Pb ratios, rather than geologically significant differences in crystallization ages. The Topawa Group and correlative units yield six U-Pb ages 178–170 Ma. The interpreted age of KPGD is 165 ± 2 Ma; those of similar granodiorite in north-central Sonora are 166 and 170 Ma. Although APQD has not been dated, its age is bracketed by those of the Topawa Group, 170 ± 3 Ma, and KPGD, 165 ± 2 Ma. Monzodiorite in Sierra La Alesna probably correlative with APQD is 164(?) Ma, suggesting that APQD and KPGD are approximately coeval. The single U-Pb age determined for PKG is 159 ± 2 Ma. BPPG is dated as 146 ± 3 Ma, and similar perthite granite near Sierra del Cobre as 149 Ma.

PETROCHEMISTRY OF KITT PEAK PLUTONIC SUITE

Alteration

Haxel et al. (2008) show that, unlike many Jurassic igneous rocks in south-central Arizona, KPPS as a whole is minimally altered. Furthermore, because our samples are from

Table 1. Interpreted U-Pb zircon isotopic ages for Jurassic igneous rock units, Comobabi-Baboquivari-Arivaca region, south-central Arizona, and adjacent north-central Sonora.

Group, Formation, or pluton[1]	Range[2]	Age (Ma)	Geochronologist; reference[3]
Middle to early Late Jurassic: main magmatic arc			
Topawa Group	Baboquivari Mountains		
Ali Molina Formation (AMF)		170 ± 3	J.E. Wright; Haxel et al., 2005
Tinaja Spring Porphyry (TSP)		≲174	" "
Kitt Peak Plutonic Suite	Baboquivari Mountains		
Kitt Peak Granodiorite (KPGD)		165 ± 2	J.E. Wright; Haxel et al., 2005
Pavo Kug Granite (PKG)		159 ± 2	" "
Las Guijas igneous suite			
Cobre Ridge Tuff (CRT) {AMF}	Cobre Ridge	170 ± 5	N.R. Riggs; Riggs et al., 1993
Las Guijas porphyry {TSP}	San Luis Mountains	174 ± 2	S.A. Bowring; Drewes, 1997
Durazno granite	Las Guijas Mountains	178 ± 3	N.R. Riggs; Spencer et al., 2003
Unnamed granite	Cobre Ridge	≥167	W.R. Premo; Drewes, 1998
Cubabi rhyolite [AMF, CRT]	Sierra del Cobre, SO	176	T.H. Anderson; Anderson et al., 2005
Sebaco monzodiorite [APQD]	Sierra La Alesna, SO	164 (?)	" "
El Plomo granite [KPGD]	Cerros del Plomo, SO	166	" "
Gabino quartz monzonite [KPGD]	Sierra La Espuma, SO	170	" "
Late Jurassic: post-magmatic arc, crustal extension			
Baboquivari Peak Perthite Granite (BPPG)	Baboquivari Mountains	146 ± 3	J.E. Wright; Haxel et al., 2005
San Moises granite [BPPG]	Sierra del Cobre, SO	149	T.H. Anderson; Anderson et al., 2005
Mount Devine perthite granite	Comobabi Mountains	158 ± 3	J.E. Wright; Haxel et al., 2008
Ko Vaya Granite	Comobabi Mtns, Santa Rosa Mtns	~150 (?)	" "

[1]For Sonoran units, probable Arizonan equivalent is specified, in brackets. For two units of the Las Guijas igneous suite, correlatives in the Topawa Group are indicated, in braces.
[2]Arizona unless designated Sonora (SO).
[3]Analytical methods: thermal-ionization mass spectrometry (TIMS); except Ali Molina Formation, Sensitive High-Resolution Ion Microprobe–Reverse Geometry (SHRIMP–RG).

undeformed rocks in which igneous textures and minerals are well preserved, effects of metamorphism also are negligible. We henceforth assume that compositions of the KPPS rocks (Table 2) are magmatic. The only exceptions are two aberrant samples, one KPGD, one PKG.

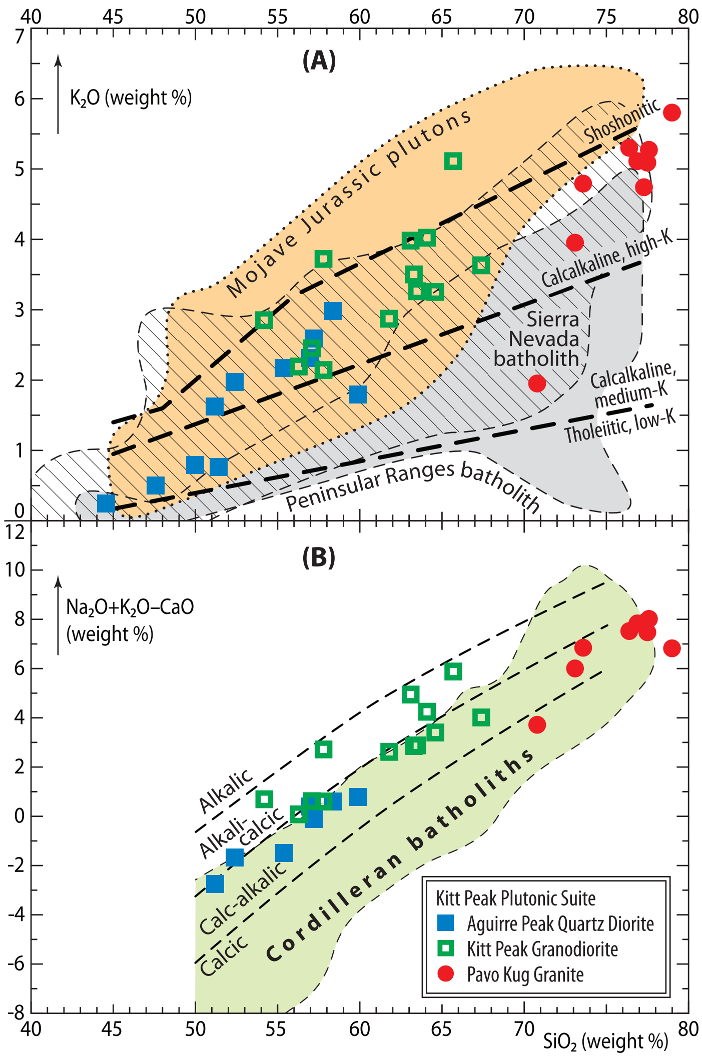

Figure 6. **(A)** Classification of the Kitt Peak Plutonic Suite in terms of SiO_2 and K_2O (Peccerillo and Taylor, 1976; Rickwood, 1989); and comparison with Jurassic plutons of the Mojave desert (Fox and Miller, 1990; Young et al., 1992; Gerber et al., 1995; Miller and Glazner, 1995; Mayo et al., 1998), Cretaceous plutons of the central Sierra Nevada batholith, California (Bateman, 1992; data from the North American Volcanic and Intrusive Rock Database [NAVDAT]: http://navdat.kgs.ku.edu/), and the Cretaceous Peninsular Ranges batholith, California (Silver and Chappell, 1988). **(B)** Comparison of KPPS with the generalized composition of Cordilleran granitoids (Frost et al., 2001); K_2O+Na_2O-CaO (ordinate) is the "modified alkali-lime index" (MALI) of those authors. Four samples of APQD have MALI ≈ –15 to –9 and thus plot below this diagram.

Table 2. Kitt Peak Plutonic Suite, representative analyses.*

Unit	APQD		KPGD	PKG
Sample	SP 134	CM 600	PR 17	BD 15
Lithology	hornblende mesodiorite	bio-hb qtz diorite	hb-bio granodiorite	biotite granite
SiO_2	50.1	57.2	61.8	76.4
Al_2O_3	11.6	16.4	17.8	13.0
Fe_2O_3	2.02	2.14	2.08	0.30
FeO	5.85	4.78	2.40	0.31
MgO	11.7	4.22	1.60	0.27
CaO	11.6	6.14	4.48	0.83
Na_2O	1.76	3.41	4.20	3.03
K_2O	0.80	2.58	2.86	5.29
TiO_2	0.77	1.00	0.64	0.13
P_2O_5	0.14	0.28	0.19	<0.05
MnO	0.15	0.13	0.09	<0.02
H_2O	1.88	1.13	0.53	0.32
F	0.03	0.10	0.05	0.02
CO_2	0.15	0.07	0.01	0.01
Total	99.2	100.2	99.2	100.0
Li	12.	30.	30.	20.
Rb	14.9	132.	88.5	294.
Cs	0.2	4.5	2.1	3.5
Be	0.7	2.0	1.6	2.9
Sr	298.	482.	442.	63.
Ba	267.	868.	1520.	209.
Sc	41.	15.	9.	1.8
Ti	4700.	6000.	4100.	800.
V	133.	178.	94.	7.
Cr	265.	79.	6.	2.
Mn	1060.	1010.	720.	190.
Co	47.0	26.1	10.1	1.3
Ni	235.	54.8	5.5	1.2
Cu	56.	50.	27.	18.
Zn	58.	120.	81.	16.
Th	2.7	7.4	7.1	24.6
U	0.44	2.78	2.27	5.74
Zr	70.9	150.	128.	46.8
Hf	2.	4.	4.	2.
Nb	4.	12.	10.	15.
Ta	<0.5	0.8	0.7	1.5
Mo	0.24	1.42	0.79	1.05
W	<0.1	0.7	0.3	1.3
Ga	13.	23.	19.	14.
In	0.06	0.06	0.05	0.03
Tl	<0.1	0.6	0.3	0.9
Ge	2.	2.	4.	2.
Sn	0.8	1.6	1.4	0.9
Pb	9.	12.	13.	18.
P	600.	1100.	1200.	100.
Sb	0.15	0.23	0.35	0.23
Bi	<0.04	0.10	0.05	0.06
S	0.03	0.02	0.02	<0.01
La	14.1	32.9	41.0	35.8
Ce	31.0	65.5	82.1	56.1
Pr	4.15	8.09	9.56	5.56
Nd	17.0	31.6	33.7	16.8
Sm	3.9	5.9	5.8	2.7
Eu	1.13	1.36	1.51	0.38
Gd	4.34	5.50	5.77	2.45
Tb	0.66	0.77	0.85	0.40
Dy	3.62	4.02	4.37	2.50
Ho	0.73	0.78	0.93	0.54
Er	2.35	2.45	2.84	2.11
Tm	0.28	0.31	0.36	0.35
Yb	1.80	2.00	2.60	2.60
Lu	0.29	0.29	0.45	0.45
Y	19.8	23.3	22.1	16.5

*Major and minor element oxides and F, weight percent; trace elements, μg/g. Analytical methods: Appendix. Total includes Fe as Fe_2O_3, SrO, BaO, and –O≙F. All four samples have Cl ≤ 0.02%.

Classification and comparison with other plutonic suites

In the standard classification in terms of SiO_2 and K_2O, the main trend for KPPS lies within the high-K calcalkaline field (Fig. 6A). APQD and KPGD plot largely in the middle of the field for Jurassic plutons of the Mojave Desert, but PKG is less potassic than Mojave Jurassic granites (in some of which elevated K_2O may owe to alteration). KPPS is distinctly more potassic than the Cretaceous Peninsular Ranges batholith, and plots in the upper half of the field for the Cretaceous central Sierra Nevada batholith. In terms of the alkali-lime index of Peacock (1931; Arculus, 2003) and Frost et al. (2001), the KPPS is transitional between calc-alkalic and alkali-calcic, and plots in the upper part of or slightly above the generalized field of Cordilleran batholiths (Fig. 6B).

APQD and most samples of KPGD are metaluminous (Fig. 7). PKG is weakly peraluminous. In contrast, the widespread early Paleogene leucogranites of southern Arizona and northern Sonora (Keith et al., 1980; Wright and Haxel, 1982; Nourse et al., 1994) are, for the most part, strongly peraluminous. This chemical contrast is expressed in the mineralogy of the two suites—the early Paleogene leucogranites contain various combinations of biotite, muscovite, and garnet whereas PKG typically has only biotite.

Behavior of trace elements

Our dataset includes analyses for some 50 trace elements (Table 2; Appendix). Abundances of several—e.g. Cs, Th, W, Sc, Co, Ni, and Cu—range over 2–2½ orders of magnitude, through the progression from mafic to silicic igneous rocks. We have systematically examined the behavior of trace elements by plotting their concentrations against indicies of igneous evolution. Indicies considered include SiO_2; FeO* (total iron as FeO), MgO, CaO, and binary sums of these; and *mg* (Fig. 8 caption). We found that FeO*+CaO generally yields the most coherent trends.

Four categories of trace element behavior can be distinguished. (1) Rb, K, Th, U, and W are consistently incompatible, increasing monotonically through the sequence from mesodiorite to leucogranite (Fig. 9A). (2) Sc, V, Cr, Co, Ni, and Cu are compatible, decreasing monotonically with igneous evolution (Fig. 9B). (3) Cs, Ba, P, Ti, Zr, Hf, Sn, LREE, MREE (including Eu), Zn, and Ga are incompatible in the earlier stages of evolution, reach maximum concentrations in intermediate rocks, and then become compatible at more evolved (more silicic) compositions. That is, these elements display markedly concave-downward trends (Fig. 9C). (4) Pb, Nb, Mo, HREE, Sb, and Bi increase from mafic to intermediate compositions, then remain semiconstant in intermediate through silicic rocks (not shown).

Concentrations of ore elements

Laramide metaluminous plutons in southern Arizona and northern Sonora are famous for their associations with numerous porphyry Cu deposits (Titley, 1995). The metallogenic potential of Jurassic plutons is less well known. In this context, we have examined abundances of several potential ore metals, and elements that might be associated with ores, in Laramide metaluminous granitoids (LMAG) of south-central Arizona and north-central Sonora and in the Jurassic KPGD and APQD (Fig. 10). We also compare Jurassic PKG with the geochemically distinctive late Laramide (early Paleogene) peraluminous leucogranites (PALG) of south-central Arizona and north-central Sonora; and compare these four Arizona-Sonora igneous suites with global average upper continental crust (UCC).

Relative to UCC, all four Arizona-Sonora suites are slightly to strongly depleted in W, Sn, and Mo. In its concentrations of the other nine elements plotted in Figure 10, KPGD+APQD closely mimics average upper crust. KPGD+APQD and LMAG, both dominated by granodiorite and granite, have generally similar patterns. However LMAG, despite its association with Cu±Mo deposits, has less than one-half as much Cu and Mo as KPGD+APQD. PALG is characterized by strong depletion in W, Mo, Sb, Zn, and Cu; and marked enrichment in Ta and Nb. PKG, also peraluminous leucogranite (Fig. 7), does not share these special features, but is notable for relatively high W and low Sn. Both leucogranites are modestly enriched in U, and PKG in Th as well.

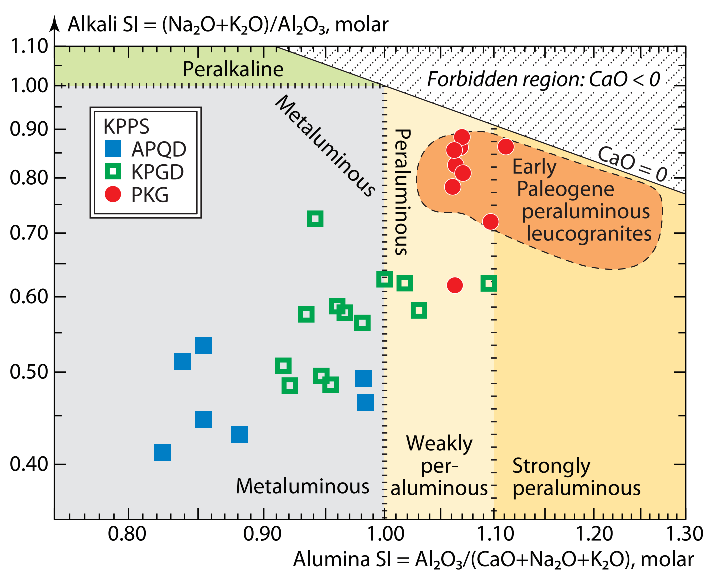

Figure 7. Alumina saturation index (Al SI) and alkali saturation index (Alk SI) in the Kitt Peak Plutonic Suite; and comparison with early Paleogene peraluminous leucogranite in south-central Arizona and north-central Sonora (103 samples: Haxel, unpublished data; Coney and Reynolds, 1980). Four other samples of APQD have Al SI ≈ 0.3–0.7 and Alk SI ≈ 0.1–0.3, and thus plot off this diagram. Axes are logarithmic so that the boundary of the forbidden region is linear.

PETROGENESIS OF KITT PEAK PLUTONIC SUITE

Petrogenetic relations of APQD, KPGD, and PKG

In binary variation diagrams (e.g., Figs. 6–9), APQD and KPGD overlap in composition and define a single smooth trend, suggesting that they are genetically related. APQD and KPGD also have very similar abundance patterns for incompatible to moderately compatible elements (Fig. 11A), virtually requiring that the two units are consanguineous. Only two minor differences in the patterns are significant—KPGD has slightly higher concentrations of the more highly incompatible elements (Cs–Ce) and slightly lower concentration of compatible elements (Ti, V, Sc). These differences are just as expected if KPGD evolved from APQD (by processes to be considered shortly). REE spectra of APQD and KPGD are similar in shape and overlap extensively (Fig. 12A), further demonstrating the close tie between these two units. This inference from geochemical data that APQD and KPGD are genetically related is consistent with geochronologic data suggesting they are coeval.

Field observations, modes (Fig. 5), and major and trace element patterns (Figs. 6, 7, 9–13) all indicate compositional discontinuity between KPGD and PKG. And, PKG is about 6±4 m.y. younger than KPGD. Nonetheless, the close spatial association of KPGD and PKG in the Baboquivari Mountains (Fig. 2) surely is not coincidental, as Jurassic KPGD-like granodiorite and PKG-like granite occur together frequently in the Sonoran-Mojave Desert region (Tosdal et al., 1989).

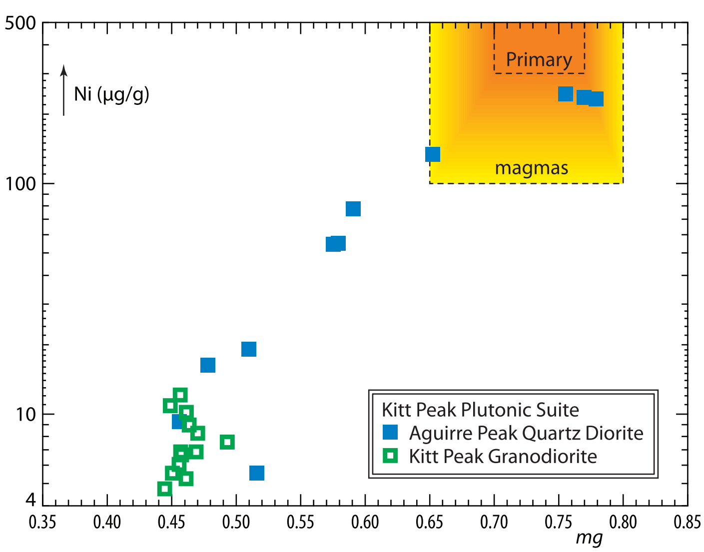

Figure 8. Mg number *(mg)* and Ni concentration in APQD and KPGD. *mg* = MgO/(MgO+FeO), molar; with weight percent $Fe_2O_3/(Fe_2O_3+FeO)$ set to 0.2. Orange to yellow rectangles respectively delineate the most and least restrictive ranges of values of *mg* and Ni generally considered indicative of primary, mantle-derived magmas (Sato, 1977; Gill, 1981; Rock, 1991; Tatsumi and Eggins, 1995; Nixon and Johnston, 1997). PKG, with *mg* ~ 0.4 and Ni ~ 3 μg/g, plots below this diagram.

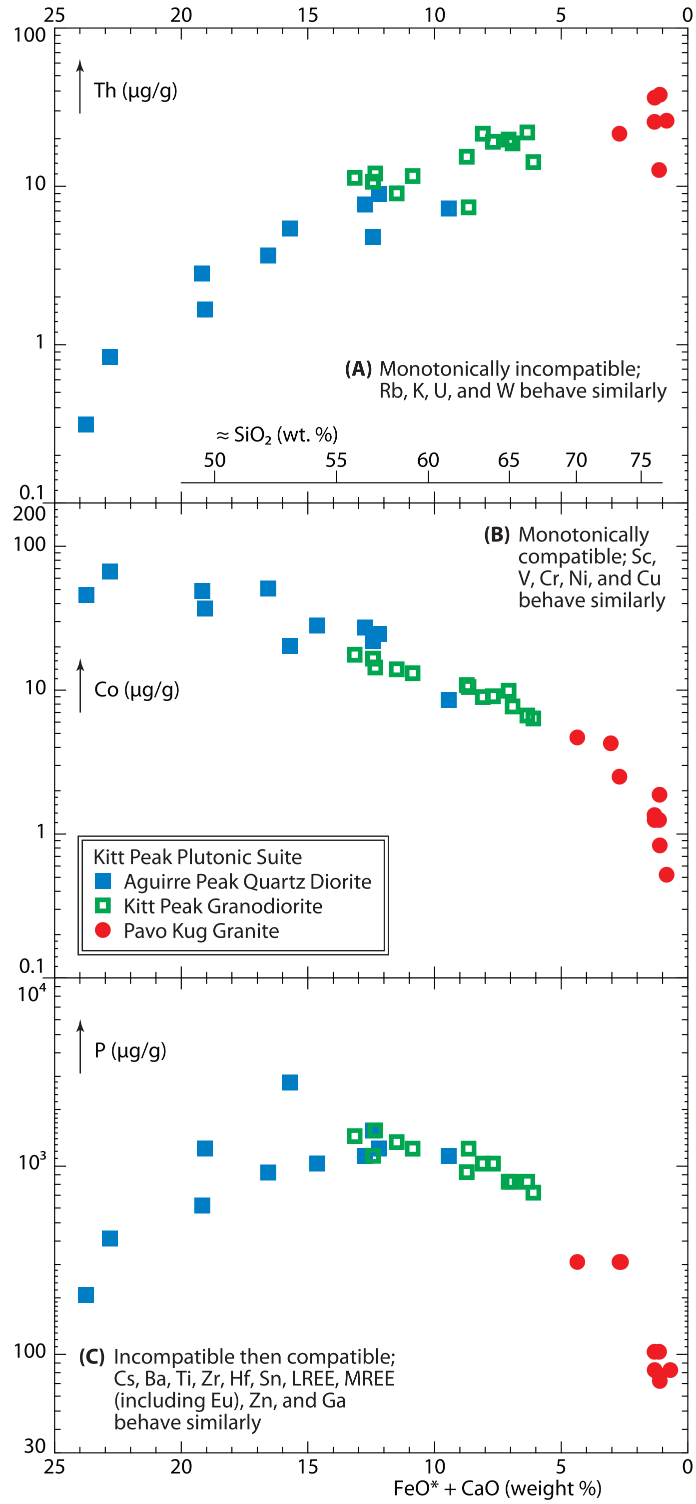

Figure 9. Typical trace element variations as a function of igneous evolution, illustrating the first three of the four types of behavior described in text. FeO*+CaO provides an evolutionary index, decreasing through the progression from mafic rocks (left side) to silicic rocks (right side). Auxiliary scale in graph (A) shows approximate equivalent SiO_2, based on polynomial regression of FeO*+CaO and SiO_2. FeO* denotes total iron as FeO.

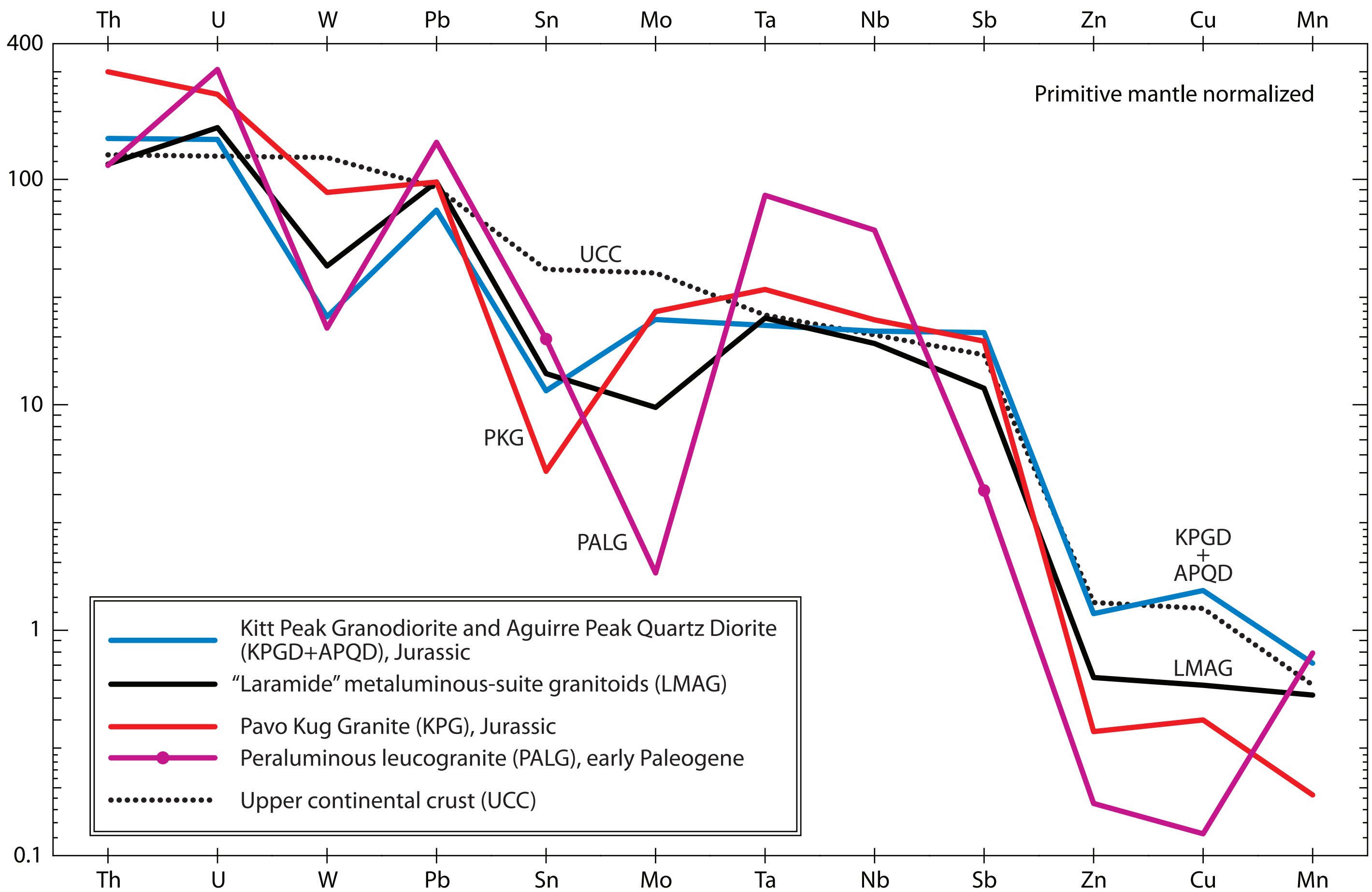

Figure 10. Average concentrations, normalized to primitive-mantle values, of 12 potential ore metals and related elements in KPGD+APQD (24 samples), PKG (9 samples), Laramide metaluminous-suite granitoids (LMAG; ≈ 14–60 samples) and peraluminous leucogranite (PALG; ≈ 26–85 samples) of south-central Arizona and north-central Sonora, and global average upper continental crust (UCC). For the Arizona and Sonora rocks, the average plotted is the median composition; except the average for KPGD+APQD is the weighted arithmetic mean of their medians. Given the much larger map area of KPGD than APQD (Fig. 2), these units are weighted 90% and 10%, respectively. Surprisingly high Mn in PALG is related to the presence of Fe-Mn garnet. Zinc in PALG is estimated from sparse data in Arnold (1986). Elements are arranged (left to right) in order of increasing compatibility in partitioning between present upper continental crust (McLennan, 2001) and the primitive mantle (Palme and O'Neill, 2005), as indicated by the ratio of concentrations in these two reservoirs. This ratio ranges from 128 for Th and U to 0.57 for Mn.

Though KPGD and PKG must be broadly related within the framework of the Jurassic magmatic arc, their petrogenetic link evidently is less direct than that between APQD and KPGD.

Identification of primary magma

In general, primary (mantle-derived) basalts are characterized by high concentrations of compatible elements such as Mg, Sc, Cr, Co, and Ni; and by high Mg/Fe, as expressed by the Mg number, $mg = MgO/(MgO+FeO)$. APQD mesodiorites are basaltic (Fig. 6A), and have compositions within the ranges considered indicative of primary magmas (Fig. 8). Furthermore, trace element patterns are much like those of primitive basalts from other continental magmatic arcs (Fig. 11B) (Kelemen et al., 2005). APQD as a whole closely resembles primitive continental-arc andesites (Fig. 11C). Thus, we infer that APQD mesodiorite approximates the composition of the primary (or at least primitive) magma of the APQD–KPGD series. This mafic magma evidently was volatile-rich, as crystallization of hornblende requires high water pressure (Burnham, 1979).

Rare earth element model

In terms of REE, igneous evolution of average KPGD granodiorite from average APQD diorite can be readily modeled by crystal fractionation of hornblende and plagioclase (Fig. 12B). The best fit is obtained with a dioritic fractionating (precipitating) assemblage comprising 27 percent hornblende and 73 percent plagioclase. An alternative assemblage of 23 percent hornblende, 77 percent plagioclase, and 0.26 percent apatite yields virtually the same result. In either case, part of the plagioclase can be replaced by other minerals with small to

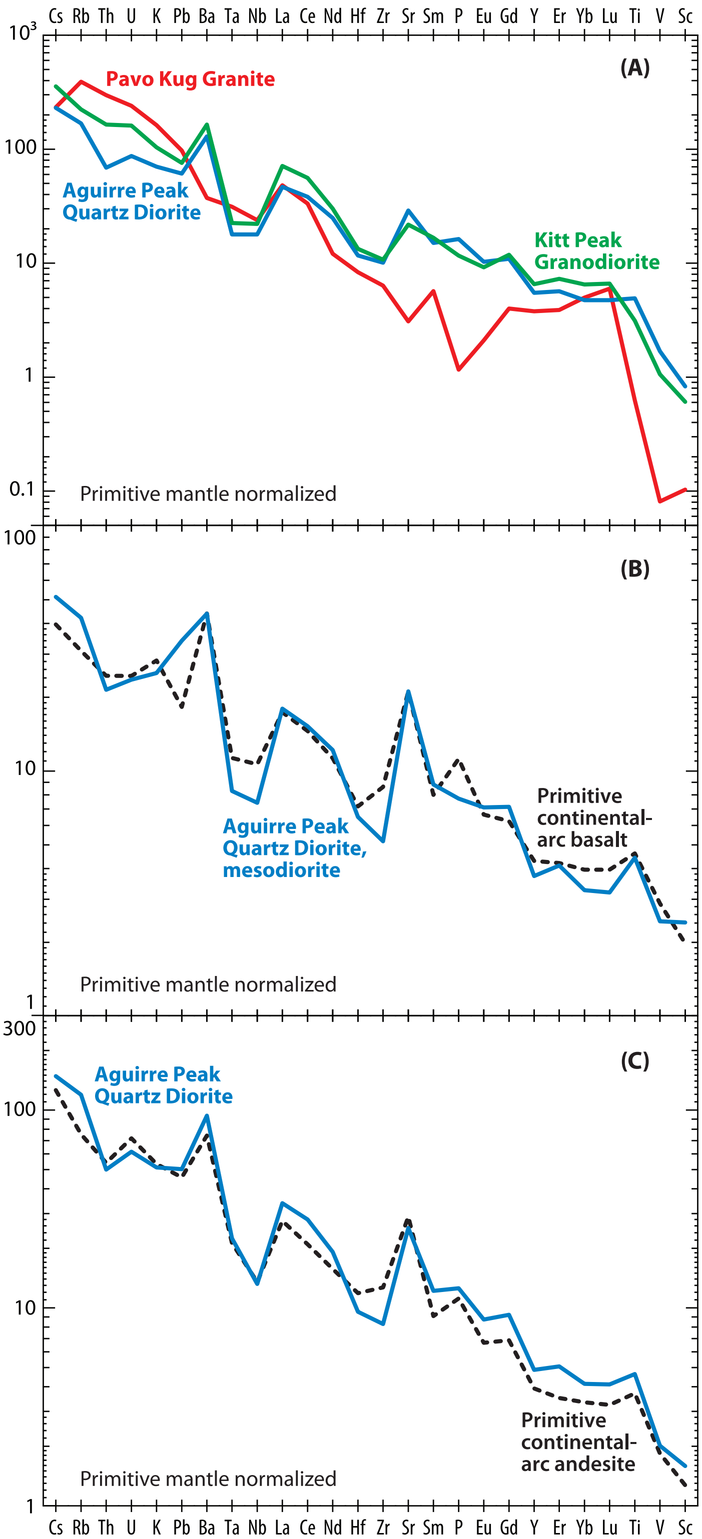

Figure 11. Average concentrations of incompatible and moderately compatible elements in **(A)** APQD, KPGD, and PKG (median concentrations); **(B)** APQD primitive mesodiorite (5 samples; arithmetic mean concentration) and primitive continental-arc basalt; and **(C)** APQD (all 11 samples; arithmetic mean concentration) and primitive continental-arc andesite. These diagrams are after Sun and McDonough (1989); primitive arc basalt and andesite are from Kelemen et al. (2005); concentrations are normalized to primitive mantle values (Palme and O'Neill, 2005).

negligible partition coefficients for all REE or all REE except Eu—specifically biotite, alkali feldspar, or quartz—without significantly improving or degrading the overall fit.

Incompatible element–compatible element model

Elementary numerical models for the petrogenesis of igneous rocks, though grossly oversimplified, have the significant advantage that they minimize the number of parameters that

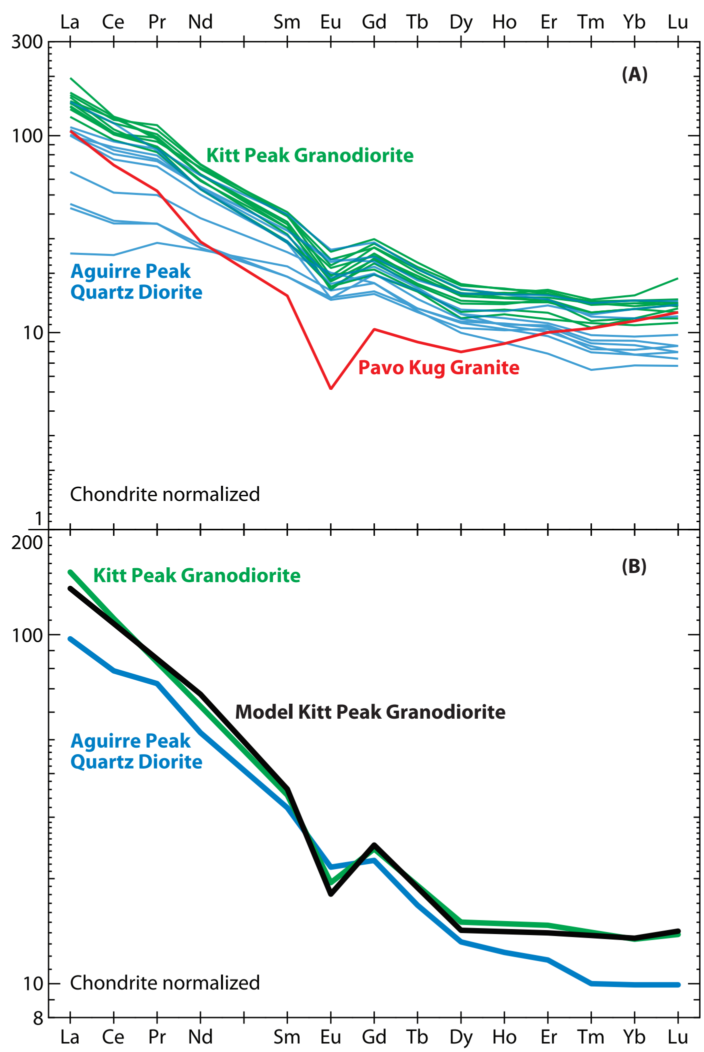

Figure 12. **(A)** Chondrite-normalized rare earth element spectra of APQD, KPGD, and PKG. Two deviant samples, one APQD and one PKG, are not plotted. For PKG only the average composition is shown, in order to avoid visual clutter. All 14 stable lanthanides were determined, by ICP (Appendix). Normalizing values from Nakamura (1974). **(B)** REE modeling of the evolution of median KPGD from median APQD by perfect fractional crystallization. The best fit is obtained with 38% crystallization of a model fractionating assemblage comprising 27% hornblende and 73% plagioclase (see text). For the ten REE modeled—La, Ce, Nd, Sm, Eu, Gd, Dy, Er, Yb, and Lu—root-mean-square deviation between model and actual KPGD is < 6%. The largest relative error for any single REE, La, is 10%. Partition coefficients from Rollinson (1993) and Sisson (1994).

have be estimated or fit to the data. Four such simple models warrant consideration before more complex models are entertained: batch partial melting, perfect fractional crystallization, binary mixing, and assimilation accompanying fractional crystallization. Equations governing these processes are given by Shaw (2006). These four petrogenetic models can be examined by plotting a highly incompatible trace element (bulk distribution coefficient, D, ≤ 0.1) as abscissa versus a compatible trace element ($D \geq 2$) as ordinate, on a logarithmic graph (Pearce, 1982) (Fig. 13). In this diagram, model magmas generated by low to moderate degrees of batch partial melting plot along a subhorizontal trend. Progressive perfect fractional crystallization generates linear arrays lying below the partial melting trend and having moderate to steep negative slopes. Mixing of mantle-derived magma with continental crust generates curves connecting these two compositions. Fractional crystallization with assimilation produces curves that, for low to moderate degrees of crystallization, typically lie between the trajectories for fractional crystallization and mixing.

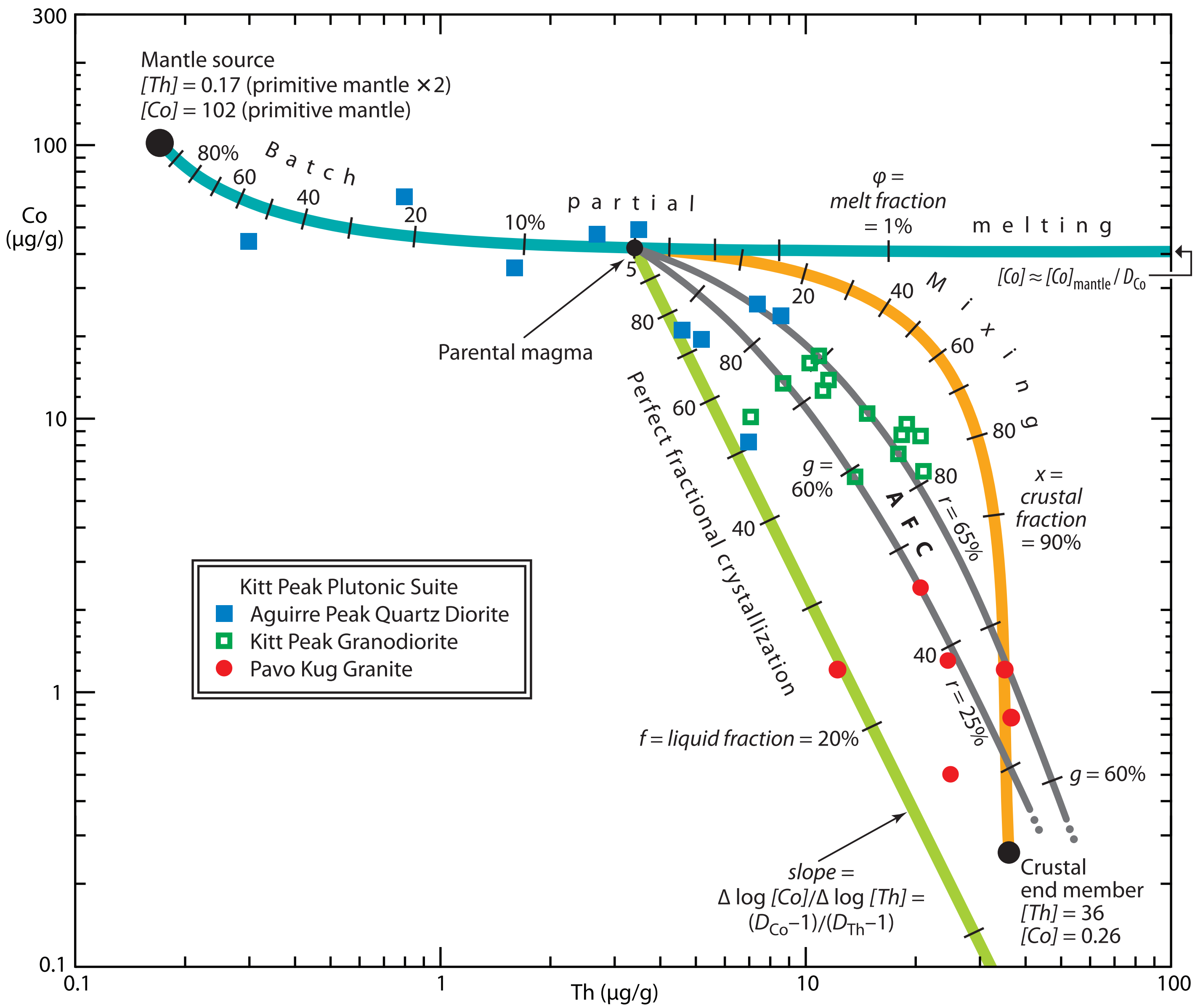

Figure 13. Numerical modeling of the petrogenesis of the KPPS, by batch partial melting, perfect fractional crystallization, mixing with continental crust, and assimilation–fractional crystallization (AFC) (Shaw, 2006). Parameters of the models are specified in Table 3, and explained in text. Brackets denote concentration, in μg/g. D_X, the bulk distribution coefficient, quantifies equilibrium partitioning of trace element X between coexisting solid and liquid: D_X = *([X] in the solid)/([X] in the liquid)*. For melting, the solid is the residual material; for crystallization, the solid is the fractionating assemblage. Variables for the partial melting (φ), fractional crystallization *(f)*, and mixing *(x)* models are defined in the graph. In the AFC model, *g* is the liquid fraction and *r* is the ratio of assimilation rate to fractional crystallization rate *(r* = 0 for perfect fractional crystallization). Each of these five variables can, in principle, range from zero to 100%. Ticks on the fractional crystallization, mixing, and AFC curves mark 10% intervals. Ticks on the melting curve mark φ = 1, 2, 3, 4, 5, and 10–90%.

In applying this plot to the KPPS, the incompatible trace element might be Rb, Th, or U. Thorium is less susceptible to post-magmatic mobility than Rb and U. The compatible element could be Sc, Cr, Co, or Ni. For the KPPS, Th and Co yield the most systematic plot. Figure 9 demonstrates that Th and Co are consistently incompatible and compatible, respectively.

The minimum number of end members involved in the petrogenesis of continental igneous rocks is two: a mantle source, which provides the parental magma, and a crustal reservoir, which contributes through mixing or assimilation. We assume the principal mantle source is subcontinental lithospheric mantle enriched in incompatible elements relative to primitive mantle (Wilson, 1989), so we take the source concentration of Th as twice that of primitive mantle. For the crustal end member, we consider two compositions. Early Paleogene peraluminous leucogranites in southern Arizona represent melts of the lower crust (Farmer and DePaolo, 1984). PKG leucogranite likewise is quite silicic and poor in Mg and Fe, and must be derived largely or entirely from the crust. The first melt or assimilate of crustal material should have the most Th and the least Co. Interestingly, early Paleogene and Jurassic (PKG) leucogranite have quite similar maximum Th and minimum Co; we use averages for these two units as the crustal end member (Table 3). Bulk distribution coefficients used are based on those for petrologically similar suites of igneous rocks described in the literature, and on the best-fit fractionating assemblage from the REE model (Table 3).

Figure 13 illustrates one plausible scenario for magmatic evolution of the KPPS. APQD primitive mesodiorites plot along a reasonable partial melting trend. The remainder of the KPPS rocks plot between a reasonable fractional crystallization line and mixing curve, and along assimilation–fractional crystallization curves for moderate rates of assimilation. Some of the scatter may owe to varying degrees of separation of liquids and crystals (McCarthy and Hasty, 1976). All of these trends converge, at their upper ends, on the composition of the model parental magma. These preliminary results suggest that simple numerical models can indeed provide insight into the petrogenesis of the KPPS. The present dataset for major and trace elements is entirely adequate to support more detailed modeling; what is needed now is more isotopic data. The single determination of radiogenic isotope composition for the KPPS—KPGD: $(^{87}Sr/^{86}Sr)_{initial} = 0.707$, $\varepsilon_{Nd} = -8.5$ (Farmer and DePaolo, 1984)—is consistent our inference that KPGD represents a mixture of mantle and lower crustal sources.

Table 3. Parameters for the petrogenetic models illustrated in Figure 13.

Parameter*	Th	Co	References
D_{mantle}	$6 \cdot 10^{-5}$	2.5	McKenzie and O'Nions, 1991; Pearce and Parkinson, 1993
D_{crust}	0.07	$3.5^{\dagger}$	Bacon and Druitt, 1988; Rollinson, 1993
conc in mantle source: Th, 2 × conc in PM; Co, conc in PM	0.17	102.	Palme and O'Neill, 2005
conc in crustal end member			
max Th, min Co in PKG	36.5	0.5	
max Th, min Co in PALG	35.7	0.135	
geometric mean	36.	0.26	

*Conc, concentration (μg/g); max, maximum; min, minimum; PM, primitive mantle; PKG, Pavo Kug Granite; PALG, early Paleogene peraluminous leucogranite, south-central Arizona and north-central Sonora.

†Assuming a fractionating mineral assemblage based on REE modeling (Fig. 12B): 27 percent hornblende, 73 percent plagioclase.

Interpretive magmatic history

Approximately 165 Ma, mantle-derived, APQD-like, volatile-rich, mafic magma ascended into the upper crust. Some of this magma crystallized to form pipes and other small intrusions of mesodiorite; some differentiated to produce stocks of quartz diorite. As the flux of mafic magma continued or increased, a much larger chamber developed, in which APQD-like magma fractionated and assimilated lower continental crust. This chamber prevented additional mafic magma from reaching the upper crust. Hybrid magma from this chamber rose into the upper crust and crystallized to form the intermediate-composition, 165-Ma KPGD pluton. Several million years later, ≈ 159 Ma, a separate(?) episode of crustal melting produced the magma that crystallized as the silicic PKG. Compositionally, PKG is affiliated with Jurassic arc magmatism, but temporally and structurally it seems to be transitional to the succeeding phase of post-arc extension-related magmatism. PKG and the oldest dated unit of the syn-extensional Ko Vaya Suite have similar U-Pb interpreted ages (Table 1). The subvertical, tabular shape of the PKG pluton (Fig. 2) may reflect intrusion along the margin of a developing Late Jurassic rift basin (Haxel et al., 2008).

Relation of the Kitt Peak Plutonic Suite to the Topawa Group

A naive view of the geologic map of the Baboquivari Mountains (Fig. 2) might suggest that the silicic, volcanic to hypabyssal Topawa Group is derived from or related to the subjacent intermediate to silicic plutonic units, KPGD and PKG. However, three lines of evidence indicate the Topawa Group and KPPS represent two distinct phases of Jurassic magmatism. First, APQD, the oldest member of the KPPS, intrudes the Topawa Group. If the silicic volcanic rocks of the Topawa Group were related to KPGD or PKG, then the Topawa Group should be younger than APQD, not older. Second, the closest compositional match for the rhyolitic Topawa Group is PKG, with $SiO_2 \geq 71$ percent. But PKG is probably about 11 m.y. younger than the Topawa Group. Third, plutonic rocks evidently associated with the Topawa Group are unlike those of the KPPS. The hypabyssal to plutonic roots of the Cobre Ridge Tuff, equivalent to the Topawa Group, are well exposed in a tilted crustal block in the Las

Guijas Mountains (Riggs and Haxel, 1990; Riggs and Busby-Spera, 1991; Drewes, 1997). If KPGD or PKG were related to the Topawa Group, then one or both of these plutonic units could be expected to underlie the Cobre Ridge Tuff. In fact, Jurassic granite in the structurally lowest level of the Las Guijas Mountains resembles neither KPGD nor PKG.

ACKNOWLEDGMENTS

Joe Briskey, Peter Coney, John Crowell, John Dillon, Keith Howard, Barbara John, Ted McKee, Steve Reynolds, Steve Richard, Nancy Riggs, Lee Silver, and Ted Theodore helped us, each in their own way, in the earlier stages of our study of the Jurassic arc in Arizona, Sonora, and California. More recently, we have learned about plutonic rocks and their alteration from Andy Barth, Mark Barton, Eric Jensen, David Johnson, Bob Kamilli, Steve Ludington, and Eric Seedorff. Dave Detra, Paul Lamothe, and Rich O'Leary guided us in obtaining and interpreting analytical data. Thanks to Tom Frost and Jon Spencer for careful reviews.

APPENDIX: ANALYTICAL METHODS

Thirty-eight samples of Jurassic plutonic rocks from the Baboquivari Mountains were analyzed for major elements (including total iron as Fe_2O_3) by wavelength-dispersive x-ray fluorescence, and for FeO, H_2O, CO_2, F, and Cl; at the laboratories of the USGS in Denver. Later, 34 of these samples were reanalyzed for some 50 trace elements (Table 2) by inductively-coupled-plasma mass spectrometry and inductively-coupled-plasma atomic-emission spectrometry (collectively, ICP); under a USGS contract with SGS Mineral Services in Toronto.

Samples analyzed by ICP are prepared by two methods, acid dissolution and sinter dissolution. In the former method, powdered rock sample is dissolved in a mixture of four inorganic acids, at 200–250° C. In the latter, rock powder is decomposed with a sodium peroxide sinter at 450° C. Acid dissolution provides lower detection limits for most elements, but does not yield quantitative data for elements—particularly Zr, Hf, and HREE—that reside partially or largely in highly refractory minerals such as zircon. Sinter dissolution completely decomposes the rock but results in generally higher detection limits (owing to a higher ratio of reagent to sample). The set of elements determined by acid dissolution and the set determined by sinter dissolution overlap considerably, necessitating a choice of data for many elements.

We have given precedence to the sinter-dissolution dataset, using it for Li, Rb, Cs, Pb, Sr, Sc, V, Co, Cu, Zn, Ga, Ge, Y, all 14 stable lanthanides (La–Lu), Th, U, Zr, Hf, Nb, Ta, and Mo. For Be, Ba, Cr, Ni, W, In, Tl, Sn, Sb, Bi, and S we have used the acid-dissolution data, because these elements were below detection in many samples prepared by sinter dissolution. Several elements in the sinter-dissolution list were below detection in a few samples, so we substituted acid-dissolution data. For example, in two of the 34 samples sinter-dissolution Pb was reported < 5 µg/g, so we substituted the acid-dissolution Pb values, 2.5 and 2.8 µg/g. Silver, Cd, As, and Te were below detection in most or all samples prepared by either method.

REFERENCES CITED

Anderson, T.H., and Silver, L.T., 1978, Jurassic magmatism in Sonora, Mexico: Geological Society of America Abstracts with Programs, v. 10, no. 7, p. 359.

Anderson T.H., Rodrîguez-Castañeda, J.L., and Silver, L.T., 2005, Jurassic rocks in Sonora, Mexico: relations to Mojave-Sonora megashear and its inferred northwestward extension, *in* Anderson, T.H., Nourse, J.A., McKee, J.W., and Steiner, M.B., editors, The Mojave-Sonora megashear hypothesis: Development, assessment, and alternatives: Geological Society of America Special Paper 393, p. 51–95.

Anderson, T.H., and Nourse, J.A., 2005, Pull-apart basins at releasing bends of the sinistral Late Jurassic Mojave-Sonora fault system, *in* Anderson, T.H., Nourse, J.A., McKee, J.W., and Steiner, M.B., editors, The Mojave-Sonora megashear hypothesis: Development, assessment, and alternatives: Geological Society of America Special Paper 393, p. 97–122.

Anonymous, no date, Carta Geologica, Tijuana: Estados Unidos Mexicanos, Secretaría de Programación y Presupuesto, Coórdinacion General de los Servicos Nacionales de Estadistica, Geographia e Informatica, Direccion General de Geographia del Territorio Nacional, escala 1:1,000,000.

Arculus, R.J., 2003, Use and abuse of the terms calcalkaline and calcalkalic: Journal of Petrology, v. 44, p. 929–935.

Arnold, A.H., 1986, Geologic implications of a geochemical study of three two-mica granites in southern Arizona: University of Arizona, M.S. thesis, 155 p.

Asmerom, Y., Patchett, P.J., and Damon, P.E., 1991, Crust-mantle interaction in continental arcs: inferences from the Mesozoic arc in the southwestern United States: Contributions to Mineralogy and Petrology, v. 107, p. 124–134.

Bacon, C.R., and Druitt, T.H., 1988, Compositional evolution of the zoned calcalkaline magma chamber of Mount Mazama, Crater Lake, Oregon: Contributions to Mineralogy and Petrology, v. 98, p. 224–256.

Barth, A.P., 1990, Mid-crustal emplacement of Mesozoic plutons, San Gabriel Mountains, California, and implications for the geologic history of the San Gabriel terrane, *in* Anderson, J.L., editor, The nature and origin of Cordilleran magmatism: Geological Society of America Memoir 174, p. 33–45.

Bateman, P.C., 1992, Plutonism in the central part of the Sierra Nevada batholith, California: U.S. Geological Survey Professional Paper 1483, 186 p.

Beikman, H.M., Haxel, G.B., and Miller, R.J., 1995, Geologic map of the Tohono O'Odham Indian Nation, southern Arizona: U.S. Geological Survey Miscellaneous Geologic Investigations Map I-2017, scale 1:125,000.

Bouse, R.M., Ruiz, J., Titley, S.R., Tosdal, R.M., and Wooden, J.L., 1999, Lead isotope compositions of Late Cretaceous and early Tertiary igneous rocks and sulfide minerals in Arizona: Implications for the sources of plutons and metals in porphyry copper deposits: Economic Geology, v. 94, p. 211–244.

Burnham, C.W., 1979, The importance of volatile constituents, *in* Yoder, H.S., Jr., editor, The evolution of the igneous rocks; fiftieth anniversary perspectives: Princeton, p. 439–482.

Carrigan, F.J., 1971, A geologic investigation of contact metamorphic deposits in the Coyote Mountains, Pima County, Arizona: University of Arizona, M.S. thesis, 67 p.

Coney, P.J., 1978, The plate tectonic setting of southeastern Arizona, *in* Callender, J.F., Wilt, J.C., and Clemens, R.E., editors, Land of Cochise; Southeastern Arizona: New Mexico Geological Society, Twenty-Ninth Field Conference, Guidebook, p. 285–290.

Coney, P.J., and Reynolds, S.J., 1980, Cordilleran metamorphic core complexes and their uranium favorability: U.S. Department of Energy, Grand Junction [Colorado] Field Office, Appendices, p. 325–627.

Cooley, M.E., 1967, compiler, Arizona highway geologic map: Arizona Geological Society, scale 1:1,000,000.

Cooper, J.R., 1971, Mesozoic stratigraphy of the Sierrita Mountains, Pima County, Arizona: U.S. Geological Survey Professional Paper 658-D, 42 p.

Davis, G.H., 1980, Structural characteristics of metamorphic core complexes, southern Arizona, *in* Crittenden, M.D., Jr., Coney, P.J., and Davis, G.H., editors, Cordilleran metamorphic core complexes: Geological Society of America Memoir 153, p. 35–77.

Dillon, J.T., 1975, Geology of the Chocolate and Cargo Muchacho Mountains, southeasternmost California: University of California, Santa Barbara, Ph.D. dissertation, 405 p.

Drewes, H., 1971, Mesozoic stratigraphy of the Santa Rita Mountains, southeast of Tucson, Arizona: U.S. Geological Survey Professional Paper 658-C, 81 p.

Drewes, H., 1976, Plutonic rocks of the Santa Rita Mountains, southeast of Tucson, Arizona: U.S. Geological Survey Professional Paper 915, 75 p.

Drewes, H.D., 1997, Geologic map of the Arivaca quadrangle and vicinity, Pima and Santa Cruz Counties, Arizona: U.S. Geological Survey Miscellaneous Field Studies Map MF-2320, scale 1:24,000.

Drewes, H.D., 1998, Geologic map of the Bartlett Mountain quadrangle, Pima and Santa Cruz Counties, Arizona: U.S. Geological Survey Geologic Investigations Series I-2624, scale 1:24,000.

Farmer, G.L., and D. J. DePaolo, 1984, Origin of Mesozoic and Tertiary granite in the western United States and implications for pre-Mesozoic crustal structure; 2. Nd and Sr isotopic studies of unmineralized and Cu- and Mo-mineralized granite in the Precambrian craton: Journal of Geophysical Research, v. 89, p. B10,141–10,160.

Ferguson, C.A., Gilbert, W.G., Pearthree, P.A., and Biggs, T.H., 2000, Geologic map of the southern Roskruge Mountains (the San Pedro and the southern half of La Tortuga Butte 7.5′ quadrangles), Pima County, Arizona: Arizona Geological Survey Open-File Report 00-06, scale 1:24, 000.

Fox, L.K., and Miller, D.M., 1990, Jurassic granitoids and related rocks of the southern Bristol Mountains, southern Providence Mountains, and Colton Hills, Mojave Desert, California, *in* Anderson, J.L. editor, The nature and origin of Cordilleran magmatism: Geological Society of America Memoir 174, p. 111–132.

Frost, B.R., Barnes, C.G., Collins, W.J., Arculus, R.J., Ellis, D.J., and Frost, C.D., 2001, A geochemical classification for granitic rocks: Journal of Petrology, v. 42, p. 2033–2048.

Gardulski, A.F., 1980, A structural and petrographic analysis of a quartzite-pegmatite tectonite, Coyote Mountains, southern Arizona: University of Arizona, M.S. thesis, 69 p.

Gerber, M.E., Miller, C.F., and Wooden, J.L., 1995, Plutonism at the interior margin of the Jurassic magmatic arc, Mojave Desert, California, *in* Miller, D.M., and Busby, C., editors, Jurassic magmatism and tectonics of the North American Cordillera: Geological Society of America Special Paper 299, p. 351–374.

Gill, J.B., 1981, Orogenic andesites and plate tectonics: Springer-Verlag, 390 p.

Gilully, J., 1956, General geology of central Cochise County, Arizona: U.S. Geological Survey Professional Paper 281, 169 p.

Goodwin, L.B., and Haxel, G.B., 1990, Structural evolution of the southern Baboquivari Mountains, south-central Arizona and north-central Sonora: Tectonics, v. 9, p. 1077–1095.

Haxel, G.B., Briskey, J.A., Rytuba, J.J., Bergquist, J.R., Blacet, P.M., and Miller, S.T., 1978, Reconnaissance geologic map of the Comobabi Mountains 15′ quadrangle, Arizona: U.S. Geological Survey Miscellaneous Field Studies Map MF-964, scale 1:62,500.

Haxel, G.B., May, D.J., Wright, J.E., and Tosdal, R.M., 1980a, Reconnaissance geologic map of the Baboquivari Peak 15′ quadrangle, Arizona: U.S. Geological Survey Miscellaneous Field Studies Map MF-1251, scale 1:62,500.

Haxel, G.B., Wright, J.E., May, D.J., and Tosdal, R.M., 1980b, Reconnaissance geology of the Mesozoic and lower Cenozoic rocks of the southern Papago Indian Reservation, Arizona: A preliminary report, *in* Jenny, J.P., and Stone, C., editors, Studies in western Arizona: Arizona Geological Society Digest 12, p. 17–29.

Haxel, G.B., May, D.J., and Tosdal, R.M., 1982, Reconnaissance geologic map of the Presumido Peak 15′ quadrangle, Arizona: U.S. Geological Survey Miscellaneous Field Studies Map MF-1378, scale 1:62,500.

Haxel, G.B., Tosdal, R.M., May, D.J., and Wright, J.E., 1984, Late Cretaceous and early Tertiary orogenesis in south-central Arizona: Thrust faulting, regional metamorphism, and granitic plutonism: Geological Society of America Bulletin, v. 95, p. 631–653.

Haxel, G.B., Wright, J.E., Riggs, N.R., Tosdal, R.M., and May, D.J., 2005, Middle Jurassic Topawa Group, Baboquivari Mountains, south-central Arizona: volcanic and sedimentary record of deep basins within the Jurassic magmatic arc, *in* Anderson, T.H., Nourse, J.A., McKee, J.W., and Steiner, M.B., editors, The Mojave-Sonora megashear hypothesis: Development, assessment, and alternatives: Geological Society of America Special Paper 393, p. 329–357.

Haxel, G.B., Anderson, T.H., Briskey, J.A., Tosdal, R.M., Wright, J.E., and May, D.J., 2008, Late Jurassic igneous rocks in south-central Arizona and north-central Sonora: Magmatic accompaniment of crustal extension, *in* Spencer, J.E., and Titley, S.R., eds., Ores and orogenesis: Circum-Pacific tectonics, geologic evolution, and ore deposits: Arizona Geological Society Digest 22, p. 333–355.

Keith, S.B., Reynolds, S.J., Damon, P.E., Shafiqullah, M., Livingston, D.E., and Pushkar, P.D., 1980, Evidence for multiple intrusion and deformation within the Santa Catalina-Rincon-Tortolita cryastalline complex, southeastern Arizona, *in* Crittenden, M.D., Jr., Coney, P.J., and Davis, G.H., editors, Cordilleran metamorphic core complexes: Geological Society of America Memoir 153, p. 217–267.

Kelemen, P.B., Hanghøi, K., and Greene, A.R., 2005, One view of the geochemistry of subduction-related magmatic arcs, with an emphasis on primitive andesite and lower crust, *in* Rudnick, R.L., Holland, H.D., and Turekian, K.K., editors, Treatise on geochemistry, v. 3, chapter 3.18: Elsevier, p. 593–659.

Knight, L.H., 1970, Structure and mineralization of the Oro Blanco mining district, Santa Cruz County, Arizona: University of Arizona, Ph.D. dissertation, 172 p.

Lang, J.R., and Titley, S.R., 1998, Isotopic and geochemical characteristics of Laramide magmatic systems in Arizona and implications for the genesis of porphyry copper deposits: Economic Geology, v. 93, p. 138–170.

May, D.J., and Haxel, G.B., 1980, Reconnaissance bedrock geologic map of the Sells 15′ quadrangle, Pima County, Arizona: U.S. Geological Survey Miscellaneous Field Studies Map MF-1166, scale 1:62,500.

Mayo, D.P., Anderson, J.L., and Wooden, J.L., 1998, Isotopic constraints on the petrogenesis of Jurassic plutons, southeastern California, *in* Ernst, W.G., and Nelson, C.A., editors, Integrated Earth and environmental evolution of the southwestern United States: Geological Society of America, p. 421–442.

McCarthy, T.S., and Hasty, R.A., 1976, Trace element patterns and their relationship to the crystallization of granitic melts: Geochimica et Cosmochimica Acta, v. 40, p. 1351–1358.

McKenzie, D., and O'Nions, R.K., 1991, Partial melt distributions from inversion of rare earth element concentrations: Journal of Petrology, v. 32, p. 1021–1091.

McLennan, S.M., 2001, Relationships between the trace element composition of sedimentary rocks and upper continental crust: Geochemistry, Geophysics, Geosystems, v. 2, paper number 2000GC000109.

Miller, J.S., and Glazner, A.F., 1995, Jurassic plutonism and crustal evolution in the central Mojave Desert, California: Contributions to Mineralogy and Petrology, v. 118, p. 379–395.

Nakamura, N., 1974, Determination of REE, Ba, Mg, Na, and K in carbonaceous and ordinary chondrites: Geochemica et Cosmochimica Acta, v. 38, p. 757–775.

Nixon, G.T., and Johnston, A.D., 1997, Nature and origin of primitive magmas at subduction zones; Preface, *in* Nixon, G.T., Johnston, A.D., and Martin, R.F., editors, Nature and origin of primitive magmas at subduction zones: Canadian Mineralogist, v. 35, p. 253–256.

Nourse, J.A., Anderson, T.H., and Silver, L.T., 1994, Tertiary metamorphic core complexes in Sonora, northwestern Mexico: Tectonics, v. 13, p. 1161–1182.

Palme H., and O'Neill, H.St.C., 2005, Cosmochemical estimates of mantle composition, *in* Carlson, R.W., Holland, H.D., and Turekian, K.K., editors, Treatise on geochemistry, v. 2, chapter 2.01: Elsevier, p. 1–38.

Peacock, M.A., 1931, Classification of igneous rock series: Journal of Geology, v. 39, p. 54–67.

Pearce, J.A., 1982, Trace element characteristics of lavas from destructive plate boundaries, *in* Thorpe, R.S., editor, Andesites; Orogenic andesites and related rocks: Wiley, p. 525–548.

Pearce, J.A., and Parkinson, I.J., 1993, Trace element models for mantle melting; application to volcanic arc petrogenesis, *in* Prichard, H.M., Alabaster, T., Harris, N.B.W., and Neary, C. R., editors, Magmatic processes and plate tectonics: Geological Society Special Publication 76, p. 373–403.

Peccerillo, R. and Taylor, S.R., 1976, Geochemistry of Eocene calc-alkaline volcanic rocks from the Kastamonu area, northern Turkey: Contributions to Mineralogy and Petrology, v. 58, p. 63–81.

Ransome, F.L., 1904, Geology and ore deposits of the Bisbee quadrangle, Arizona: U.S. Geological Survey Professional Paper 21, 167 p.

Reynolds, S.J., 1980, Geologic framework of west-central Arizona, *in* Jenny, J.P., and Stone, C., editors, Studies in western Arizona: Arizona Geological Society Digest 12, p. 1–16.

Reynolds, S.J., and Spencer, J.E., and DeWitt, E., 1987, Stratigraphy and U-Th-Pb geochronology of Triassic and Jurassic rocks in west-central Arizona, *in* Dickinson W.R., and Klute, M.A., editors, Mesozoic rocks of southern Arizona and adjacent areas: Arizona Geological Society Digest 18, p. 65–80.

Richard, S.M., Reynolds, S.J., Spencer, J.E., and Pearthree, P.A., compilers, 2000, Geologic map of Arizona: Arizona Geological Survey Map 35, scale 1:1,000,000.

Rickwood, P.C., 1989, Boundary lines within petrologic diagrams which use oxides of major and minor elements: Lithos, v. 22, p. 247–263.

Riggs, N.R., and Busby-Spera, C.J., 1991, Facies analysis of an ancient, dismembered, large caldera complex and implications for intra-arc subsidence: Middle Jurassic strata of Cobre Ridge, southern Arizona, USA: Sedimentary Geology, v. 74, p. 39–68.

Riggs, N.R., and Haxel, G.B., 1990, The Early to Middle Jurassic magmatic arc in southern Arizona: plutons to sand dunes, *in* Gehrels, G.E., and Spencer, J.E., editors, Geologic excursions through the Sonoran Desert region, Arizona and Sonora: Arizona Geological Survey Special Paper 7, p. 90–103.

Riggs, N.R., Mattinson, J.M., and Busby, C.J., 1993, Correlation of Jurassic eolian strata between the magmatic arc and the Colorado Plateau: New U-Pb geochronologic data from southern Arizona: Geological Society of America Bulletin, v. 105, p. 1231–1246.

Rock, N.M.S., 1991, Lamprophyres: Van Nostrand Reinhold, 285 p.

Rollinson, H.R., 1993, Using geochemical data; evalution, presentation, interpretation: Longman, 352 p.

Sage, L., and Ashenbrenner, G., 2003, Visitor's guide to the Kitt Peak observatories: Cambridge, 104 p.

Sato, H., 1977, Nickel content of basaltic magmas: identification of primary magmas and a measure of the degree of olivine fractionation: Lithos, v. 10, p. 113–120.

Shaw, D.M., 2006, Trace elements in magmas; A theoretical treatment: Cambridge, 243 p.

Silver, L.T., 1974, Precambrian and "Precambrian(?)" crystalline rocks of the southwestern Basin and Range province of California and Arizona: Geological Society of America Abstracts with Programs, v. 6, no. 3, p. 253–254.

Silver, L.T., and Chappell, B.W., 1988, The Peninsular Ranges batholith: an insight into the evolution of the Cordilleran batholiths of southwestern North America: Transactions of the Royal Society of Edinburgh, Earth Sciences, v. 79, p. 105–121.

Sisson, T.W., 1994, Hornblende–melt trace-element partitioning measured by ion microprobe: Chemical Geology, v. 117, p. 331–344.

Spencer, J.E., Isachsen, C.E., Ferguson, C.A., Richard, S.M., Skotnicki, S.J., Wooden, J., and Riggs, N.R., 2003, U-Pb isotope geochronologic data from 23 igneous rock units in central and southeastern Arizona: Arizona Geological Survey Open-File Report 03-08, 40 p.

Sun, S.-S., and McDonough, W.F., 1989, Chemical and isotopic systematics of oceanic basalts: implications for mantle compositions and processes, *in* Saunders, A.D., and Norry, M.J., editors, Magmatism in the ocean basins: Geological Society of London Special Publication 42, p. 313–345.

Tatsumi. Y., and Eggins, S., 1995, Subduction zone magmatism: Blackwell, 211 p.

Titley, S.R., 1995, Geological summary and perspective of porphyry copper deposits in southwestern North America, *in* Pierce, F.W., and Bolm, J.G., editors, Porphyry copper deposits of the American Cordillera: Arizona Geological Society Digest 20, p. 6–20.

Tosdal, R.M., Haxel, G.B., and Wright, J.E., 1989, Jurassic geology of the Sonoran Desert region, southern Arizona, southeastern California, and northernmost Sonora: construction of a continental-margin magmatic arc, *in* Jenny, J.P., and Reynolds, S.J., editors, Geologic evolution of Arizona: Arizona Geological Society Digest 17, p. 397–434.

Tosdal, R.M., Haxel, G.B., Anderson, T.H., Connors, C.D., May, D.J., and Wright, J.E., 1990, Highlights of Jurassic, Late Cretaceous to early Tertiary, and middle Tertiary tectonics, south-central Arizona and north-central Sonora, *in* Gehrels, G.E., and Spencer, J.E., editors, Geologic excursions through the Sonoran Desert region, Arizona and Sonora: Arizona Geological Survey Special Paper 7, p. 76–88.

Wilson, E.D., 1960, Geologic map of Yuma County, Arizona: Arizona Bureau of Mines, scale 1:375,000.

Wilson, E.D., Moore, R.T., and O'Haire, R.T., 1960, Geologic map of Pima and Santa Cruz Counties, Arizona: Arizona Bureau of Mines, scale 1:375,000.

Wilson, E.D., Moore, R.T., and Cooper, J.R., 1969, Geologic map of Arizona: Arizona Geological Survey and U.S. Geological Survey, scale 1:500,000.

Wilson, M., 1989, Igneous petrogenesis: Chapman and Hall, 466 p.

Wright, J.E., and Haxel, Gordon, 1982, A garnet-two-mica granite, Coyote Mountains, southern Arizona: Geologic setting, uranium-lead isotopic systematics of zircon, and nature of the granite source region: Geological Society of America Bulletin, v. 93, p. 1176–1188.

Young E.D., Wooden, J.L., Shieh, Y.-N., and Faber, D., 1992, Geochemical evolution of Jurassic diorites from the Bristol Lake region, California, USA, and the role of assimilation: Contributions to Mineralogy and Petrology, v. 110, p. 68–86.